

See discussions, stats, and author profiles for this publication at: <https://www.researchgate.net/publication/265849709>

Research Progress and Model Development of Crystal Layer Growth and Impurity Distribution in Layer Melt Crystallization: A Review

ARTICLE in INDUSTRIAL & ENGINEERING CHEMISTRY RESEARCH · AUGUST 2014

Impact Factor: 2.59 · DOI: 10.1021/ie5009508

CITATIONS

3

READS

45

4 AUTHORS, INCLUDING:



Xiaobin Jiang

Dalian University of Technology

22 PUBLICATIONS 104 CITATIONS

[SEE PROFILE](#)



Mo Li

ETH Zurich

7 PUBLICATIONS 13 CITATIONS

[SEE PROFILE](#)



Gaohong He

Dalian University of Technology

111 PUBLICATIONS 1,335 CITATIONS

[SEE PROFILE](#)

Research Progress and Model Development of Crystal Layer Growth and Impurity Distribution in Layer Melt Crystallization: A Review

Xiaobin Jiang,^{*,†} Mo Li,[†] Gaohong He,[†] and Jingkang Wang[‡]

[†]State Key Laboratory of Fine Chemicals, R&D Center of Membrane Science and Technology, School of Chemical Engineering, Dalian University of Technology, Dalian 116024, People's Republic of China

[‡]National Engineering Research Center of Industrial Crystallization Technology, School of Chemical Engineering and Technology, Tianjin University, Tianjin 300072, People's Republic of China

Supporting Information

ABSTRACT: Layer melt crystallization has been widely utilized in numerous chemical industries because of its high selectivity for pure products, low energy consumption, and the convenience to industrialization. This review will lay out the research progress and process model development of the key processes (crystal layer growth and impurity distribution) involved in layer melt crystallization. First, the nucleation mechanism, the preparation approaches of the initial crystal layer, and classic experimental configurations are illustrated. Second, modeling approaches are outlined to release the progress of separation effect evaluation, parameter optimization, and sweating process simulation in layer melt crystallization. Novel theories (fractal, porous media, and so on) and technologies (gradient freezing, sonocrystallization, and so forth) with suitable interpretation are potential solutions for the shortcomings of the current process research. Consequently, application areas related to layer melt crystallization are highlighted. Finally, the key issue for further research, challenges, and perspectives will be concluded.

1. INTRODUCTION

Layer melt crystallization is considered as a potential green, highly selective separation technology because of the following advantages: high selectivity for pure products; no gaseous phase; no recovery of solvents; low energy consumption (compared to distillation); easy to perform on an industrial scale.^{1–3} Considering the advantages of engineering application, layer melt crystallization (also mentioned as fractional crystallization in some areas)⁴ has been widely applied to hyperpure chemical production,⁵ ionic liquid purification,⁶ water treatment,^{7–10} nuclear engineering^{11–13} and food industry,^{14–16} etc. Moreover, hybrid distillation/melt crystallization,¹⁷ the ultrasound-assisted crystallization^{15,16,18,19} and other coupling processes have been designed to meet the requirement in various industrial areas, which explored quite promising application areas of layer melt crystallization.

To achieve the desired separation effect of melt crystallization, two key processes call for the most attention: crystal layer growth and impurity distribution (which involves the impurity entrapment and migration). These two processes are very closely correlated. The impurity (usually a solute in the liquid phase) is entrapped and migrated during the crystal layer growth. The process of crystal layer growth and the structure of the crystal layer determine the extent of impurity entrapment and the resistance of impurity migration.

The following topics should raise wide attention: the initial nucleation and layer adhering on cooled surfaces of the crystallizer were rarely evaluated comprehensively in current research, which had a profound and lasting impact on the crystal layer growth and impurity separation. What's more, different from the crystal engineering, the overall crystal layer growth rate and multicomponent impurity distribution kinetic is the key concern in layer melt crystallization model research.

In addition, impurity inclusion in the crystal layer and the molten sweating liquid migration processes are complex and influenced by the operational conditions and the initial crystal layer property. Research on the sweating process^{11,20,21} as the additional purification steps have obtained dramatic progress. Besides, the kinetics of the sweating process is also an attractive topic because of the complex structure of the crystal layer and the complicated driving force analysis.

Thus, the experimental and model research on the crystal layer growth focus on how the operational conditions impact on the manufacture efficiency of the crystal product. The research on the impurity distribution focus on the impurity distribution during the crystal layer growth and the impurity migration during the following sweating processes, all of which determine the terminal separation efficiency of layer melt crystallization. Unlike the theoretical calculation by using the solid–liquid phase diagram of the mixture, the practical purification potential depends on many critical operational conditions (nucleation, crystal layer growth, the solid–melt separation, and additional purification steps, such as sweating and washing).²² It demonstrates that proper mathematical model development supplemented by rigorous experimental validation would be an efficient and, of course, low-cost strategy for the industrial design and optimization of melt crystallization. Meanwhile, the introduction of a novel theory has been proved to be beneficial to the model development.

Traditionally, layer melt crystallization has two basic operation modes: the static melt crystallization (SMC, in

Received: March 6, 2014

Revised: July 30, 2014

Accepted: August 3, 2014

Published: August 4, 2014



Table 1. Supercooling Degree Utilized for Nucleation in Layer Melt Crystallization

crystallization system	seed	$\Delta T, K^a$	$\Delta T/T^*{}^b$	ref
acetic acid/water	no	2.4	0.009	5
water/NaCl	no	4.3	0.016	25
pure caprolactam	no	24.5	0.071	26
caprolactam/water	no	9.5	0.028	26
adipic acid ($C_6H_{10}O_4$)/hydroquinone ($C_6H_6O_2$) /water	no	2	0.006	27
benzene/ <i>p</i> -xylene	no	~25	0.082	28
α -nitrotoluene/ <i>m</i> -nitrotoluene	no	~19	0.065	28
benzene/paraldehyde	no	~26.5	0.086	28
caprolactam/water	no	15	0.043	29
isomeric long-chain aldehydes dodecanal/2-methylundecanal	no	16.5	0.058	30
acetic acid/water	yes	0.5	0.0018	31
phosphoric acid/water/acetic acid/nitric acid/Al, Fe ions	yes	0.4	0.0015	32
phosphoric acid/water/Mg, As, Sb, Pb ions	yes	0.2	0.0006	33

^a ΔT = supercooling degree. ^b $\Delta T/T^*$ = relative supercooling degree.

which only natural convection influences the mass and heat transfer) and dynamic melt crystallization (the most common mode is falling film melt crystallization, FFMC, in which forced convection is obtained by pumping the feed liquid as a falling film on a cooling surface). Note that these two modes have been proposed and widely applied and have caused considerable influence on chemical engineering manufacture.²³ The particular process characteristics, advantages, and shortcomings should be reviewed. In addition, gradient freeze technology is considered as a special layer melt crystallization applied in various relevant fields (theoretical layer growth research, food freezing, and so on).

Therefore, a scientific overview whose intention is not to focus on a single new and limited subset of results but to evaluate the overall research process is vitally necessary. In this review, a brief overview of the initial nucleation and layer adhering process would be outlined based on the classical crystallization theory. Typical melt crystallization configurations and the layer growth models proposed and developed are presented. (For more comprehensive information, readers are referred to the excellent work by Ulrich and Glade²⁴) The models which revealed the combined contribution of multiple operational conditions on the layer growth rate and temperature distributions along the crystal tower in various scales will be highlighted.

The efforts on the model of the impurity distribution (impurity entrapment and migration) then will be introduced to release the development of separation effect evaluation, operational parameter determination, and sweating process research in layer melt crystallization. A concise introduction to interruption of the kinetics of impurity migration is provided. The advantages and shortcomings of the preceding models are also discussed.

The latest findings and explored applications of layer melt crystallization are outlined, including the novel fractal theory, the ultrapure product purification and specific separation, the investigate technology in the polymeric system, gradient frozen and ultrasonic technology in the food industry, and other fields, etc. Finally, we propose our perspectives on future development and the key issues of the model development and research direction in layer melt crystallization.

2. RESEARCH PROGRESS AND MODEL DEVELOPMENT ON CRYSTAL LAYER GROWTH IN LAYER MELT CRYSTALLIZATION

2.1. Nucleation in Layer Melt Crystallization. Different from the solution crystallization (cooling crystallization, antisolvent crystallization, and so on), commonly industrial configurations of melt crystallization are towers with parallel tubes. Because of this, it is difficult to add and disperse crystal seeds. If seeds added are not distributed evenly along the tower, unsatisfactory crystal layer growth may result in tube blocking, which will render the plant inoperable or increase the separation difficulty of postprocess. The most common method to activate the nucleus is implementing a high supercooling degree on the cold tube surface without seeds. Some supercooling degrees in the layer melt crystallization reported are listed in Table 1.

As included by Kashchiev and van Rosmalen,³⁴ homogeneous nucleation (HON) occurs only in the ideally pure solutions that are constituted of solvent and solute. Heterogeneous nucleation (HEN) takes place in solutions containing impurity and/or foreign microparticles or substrates that provide active centers for nucleation. The nucleation in layer melt crystallization belongs to HEN on a substrate (Figure 1B,C). BaSO₄ is taken as an example; the kinetic nucleation parameter A ($m^{-3}s^{-1}$) of HON is 10–12 orders of magnitude (10^{10} – 10^{12}) greater than that of HEN. Calculated nucleation work of HON is twice greater than that of HEN.^{34,35} It indicates that the active centers have a prominent impact on the increase of the nucleation opportunity. For instance, Haasner et al. had proposed the effect of surface property on the

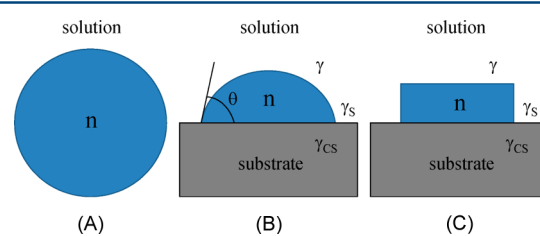


Figure 1. Cross-section of (A) spherical, (B) cap-shaped, and (C) disk-shaped cluster of n molecules during (A) HON, (B) 3D HEN, and (C) 2D HEN on a substrate (n , number of solute molecules; θ , contact angle; γ , specific surface energy of the cluster/solution interface).

nucleation zones and cost optimization of commercial layer melt crystallization processes.³⁶

This is a rapier to the operation of layer melt crystallization: compared to HON, HEN requires a smaller supercooling degree and lower energy consumption. In addition, the HEN nucleation occurs much slower than that of HEN due to the difference between their kinetic nucleation parameter A , which makes HEN nucleation more controllable and helpful for the nucleus to grow bigger with good crystal habit. The nucleation work is so small that the nucleation process will be highly sensitive to the impurity, which will inevitably increase the operational difficulty of melt crystallization. The existence of various impurities in HEN may activate or hinder the nucleation. As reported by Dang et al.,^{37,38} the nucleation work of phosphoric acid hemihydrate varied when Fe^{2+} or SO_4^{2-} was added and the metastable zone width was clearly influenced, which increased from 2.40 K (pure material) to 2.95 K (addition of SO_4^{2-} , 2100 ppm) or 3.90 K (addition of Fe^{2+} , 1500 ppm). An explanation based on the surface binding energy theory (defined as the interaction energy between an additive molecule and a specific crystal surface) had been illustrated through binding energy theory.³³ This phenomenon is not ignorable in the 2D HEN of melt crystallization. It also explains that the utilized supercooling degree should be great enough to ensure the nucleation occurs. Obviously, the nucleation rate increasing with the high supercooling degree will lead to an undesirable basal crystal layer. As shown in Figure 2, two basal crystal layers grown under different relative

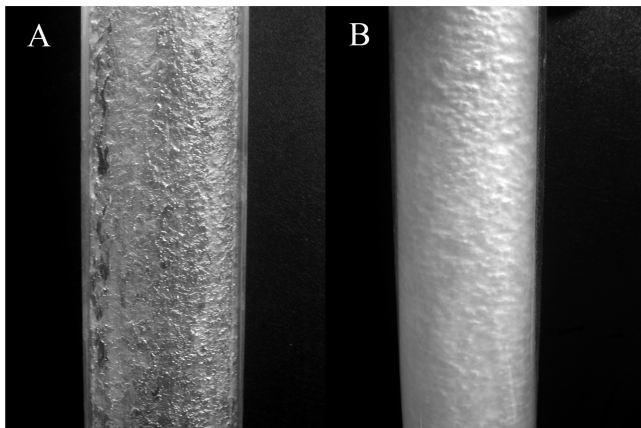


Figure 2. Comparison on two basal crystal layers grown under different relative supercooling degrees ((A) $\Delta T/T^* = 0.005$; (B) $\Delta T/T^* = 0.023$.).

supercooling degrees had quite a different appearance and thickness. In addition, the mass fraction of impurity in the right basal crystal layer (Figure 2B) was six times greater than that of the left one (Figure 2A).

Reliable nucleation method should be developed to substitute HEN. An alternative approach is adding crystal slurry as crystal seeds source onto the cooling surface by a well-designed sparger implemented on the top of the crystal tower, especially in dynamic layer melt crystallization. The slurry should meet the following requirements: (1) the slurry should be dispersed with the appropriate size and number of nuclei to avoid tubes blockage; (2) the viscosity and suspension density of the slurry should be as low as possible so that the slurry disperses evenly on the cooling surface. The commonly preparation approach of seed slurry involves rapid supercooling

operation. Meanwhile, ultrasonic method has been declared as an effective intentional seeding technology in batch crystallization. More detailed review and prospective of this topic will be found in section 4 (for more information, readers are referred to the excellent series work by Narducci and Jones^{39–42}).

2.2. Theory on Crystal Layer Growth and Research Configurations. The crystal layer grown in layer melt crystallization could be generally divided into three regions (as shown in Figure 3) presented by Scholz et al.⁴³ Region 1 is

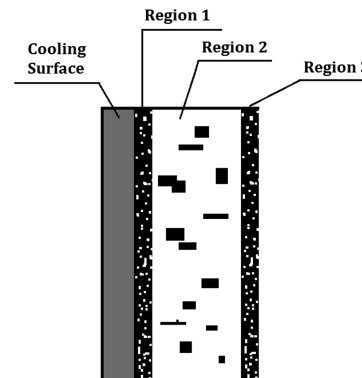


Figure 3. Illustration of different layer characteristics in solid layer crystallization. Reproduced with permission from ref 44. Copyright 2013 Elsevier.

closed to the cooling surface and has a relatively high porosity of the crystal layer in this region owing to the rapid growth rate of the crystal. When the layer growth occurs, the structure of region 2 (which is less porous than that of region 1) forms with the decreasing temperature gradient. Region 3 is the crystal layer growth frontier, and it directly contacts with the liquid phase. As an ideal crystal layer, the thicknesses of regions 1 and 3 are thin and negligible, which is also an assumption commonly employed in the model definition. The majority of impurities are enriched in region 2 and migrate during the purification process (sweating or washing). Thus, the key issues of crystal layer growth are limiting the formation of regions 1 and 3 and keeping the impurity in region 2 well-distributed, which will relieve the burden of the sweating or washing process. Of course, the crystal layer should grow under a desired rate to meet the efficient and economical requirement of industrial crystallization.

Different melt crystallization processes are implemented with various configurations. Considering the melt crystallization involving crystal layer growth, the two basic operation modes (static melt crystallization, SMC and dynamic melt crystallization or falling film melt crystallization, FFMC) will be overviewed. Dynamic melt crystallization shows advantages of continuous or semicontinuous operation and high thermal economic efficiency.²⁹ More and more plants adopt dynamic mode due to the outstanding separation effect. However, SMC also has its own advantage: the simple devices and high operational stability with fewer operational parameters. Some typical experimental configurations utilized in layer melt crystallization research are shown in Figure 4–6.

In Figure 4, the setup could carry out both SMC and FFMC processes with melt distributor on the top of the crystallizer. Two thermostatic baths are employed to provide the supercooling degree. In the FFMC process, the feed is pumped

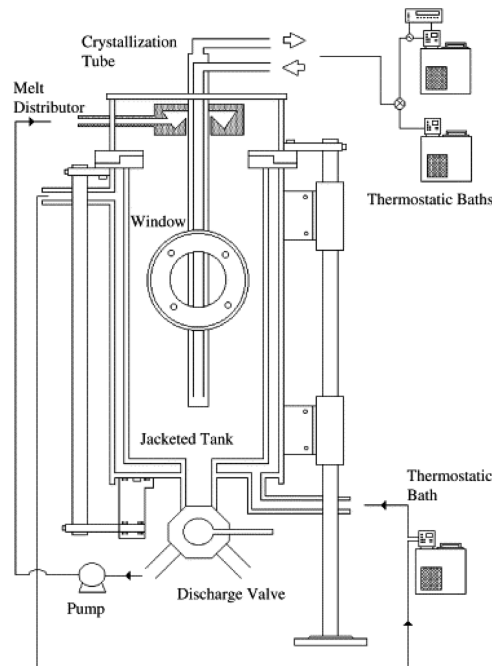


Figure 4. Schematic view of the laboratory melt crystallizer (with a melt distributor on the top the crystallizer). Reproduced with permission from ref 29. Copyright 2001 Elsevier.

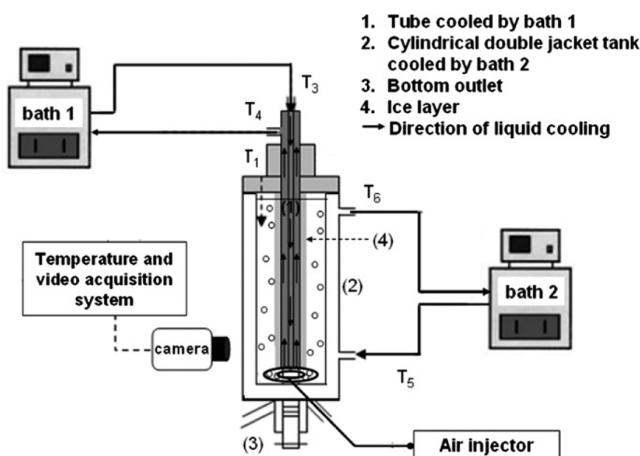


Figure 5. Experimental setup for seawater desalination by dynamic melt crystallization. Reproduced with permission from ref 25. Copyright 2012 Elsevier.

on the top of the crystallizer and dispersedly added on the cooling tube surface. In the SMC process, the feed is added into the crystallizer (which is a cylindrical double jacketed tank) and the inner cooling tube and the outer jacket of the crystallizer (which are all connected to the thermostatic baths) could establish a steady temperature gradient as the driving force of layer growth. The noncrystallized fluid could discharge from the bottom valve. A window on the crystallizer is advantageous to the layer growth measurement. This kind of setup has been applied by some researchers.^{5,29,45–47}

The experimental configuration with the air injector at the bottom (shown in Figure 5) was recently applied to seawater distillation process.²⁵ The solution in the crystallizer is agitated by air bubbling. Air recycling can reduce the energy consumption by 12% for the cooling step of 5 h, for instance. A simplified melt crystal tower was also reported in industrial

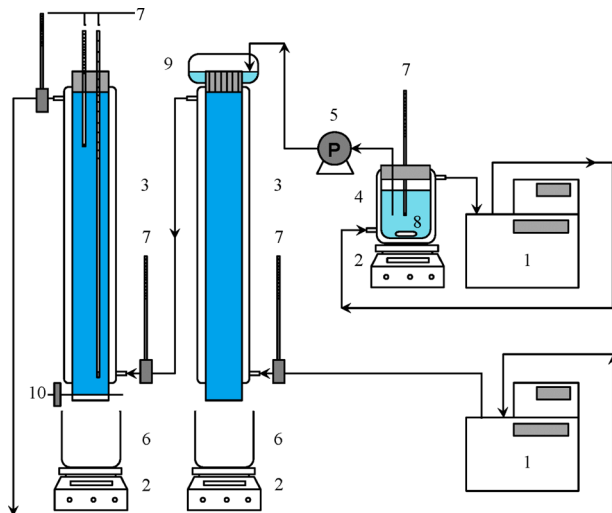


Figure 6. Schematic diagram of experimental apparatus for comparison of static (left tower) and dynamic (right tower) melt crystallization: (1) circulator bath, (2) balance with magnetic stirrer, (3) crystal tower, (4) stock tank, (5) pump, (6) beaker, (7) thermometer, (8) stir bar, (9) sparger, and (10) valve.

application.^{32,48,49} Other than the configurations mentioned above, the inner tube is not implemented and the crystal layer grows on the inner surface of the cylindrical double jacketed tower (shown in Figure 6). This kind of experimental configuration is similar to the industrial plants. Two crystal towers (one for SMC process; the other one for FFMC process) are connected in parallel and controlled by the same thermostatic bath. Thus, the operation temperature profile during static and dynamic processes can be kept simultaneously. The temperature of feed material is controlled by an independent thermostatic bath. The mass balance is performed by the balances under each towers' outlet at the bottom. The layer crystallization system with recirculation proposed by Zhou et al.,⁵⁰ which is similar to that shown in Figures 4 and 5, has an inner cooling tube and an outer cylindrical jacketed tank. The inner cooling tube is wrapped in stainless steel wire mesh, which is helpful for heterogeneous nucleation. As a system with the recirculation loop, the solute concentration at the entrance of the crystallizer is the same as that from the exit of the crystallizer. The time delay is negligible because of the small residence time in the recirculation loop. The experimental results manifest that the crystal layer thickness can be kept spatially uniform when there is no mixing in the recirculation loop.

In fact, no matter whether the SMC or FFMC process, the appropriate length-diameter ratio of the crystallizer is helpful to maintaining the high thermal economical efficiency and the separation efficiency. With regard to FFMC, the melt distributor (or sparger) on the top of the crystallizer should be well-designed to spread the feed liquid evenly. With regard to SMC, an affiliated heater might be necessary in order to avoid the crystal block at the bottom valve. In addition, affiliated measuring and investigating equipment with high accuracy and convenience should be improved, such as the temperature and video acquisition system which is connected to a camera (shown in Figure 5). The crystallizers equipped with novel detective devices are contributing to a high-accuracy control strategy and operational profiles of nucleating and crystal layer growth process.

To investigate coarse crystal layer growth and impurity distribution process of layer melt crystallization with gradient freeze technology, the experimental apparatus proposed by Jiang et al.⁵¹ is shown in Figure 7. There are two valves at the

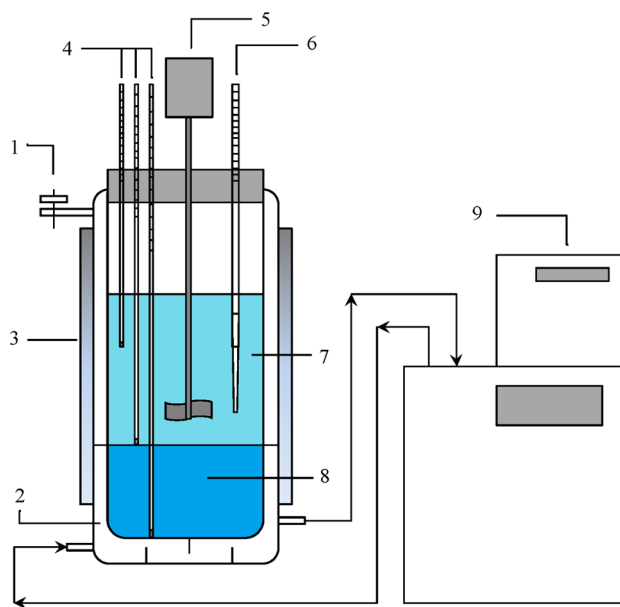


Figure 7. Schematic diagram of experimental apparatus for measuring distribution coefficients of trace amount ions with gradient freeze technology: 1, valve; 2, cooling medium; 3, crystallizer with external thermal insulation membrane; 4, thermometer; 5, stirrer; 6, probe tube; 7, phosphoric acid aqueous solution; 8, hemihydrate phosphoric acid coarse crystal layer; 9, thermostatic water bath with temperature controller.

top and bottom of the jacketed crystallizer to control the pressure in the jacket and the coolant flow rate, respectively. With the help of these two valves, a coarse crystal layer keeps growing as flat as possible during the experiment. The measured data are significantly important to the theoretical research of the impurity distribution on the crystal–liquid interface, which will be noted in section 3 in detail.

2.3. Model of Crystal Layer Growth. Crystallization processes are commonly designed on the basis of experiments that cost considerable time and money. Concerned definitions include the state of nonequilibrium, the equilibrium and growth shapes of crystals, and the surface energy, etc.⁵² Thus, mathematical models for the relevant process in the crystallization process are essential to increase the effectiveness of the process development. The model configuration of SMC had been reported by many researchers.^{26,29,30,45} As a key element in this case, the model establishment of FFMC and SMC (shown in Figure 8) was reported by Jiang et al.⁵³ As a dynamic process, the initial crystal layer grew on the inner cold surface; the falling liquid film flows over the growth frontier of the crystal layer, which is consistent with the experimental setup shown in Figure 6.

Based on the mass and heat transfer balance and the assumptions, several meaningful models of crystal layer growth in melt crystallization have been proposed. The fundamental equations and issues of these models are listed in Table 2 (the nomenclature of each model had been unified for a clear expression). It is obvious that most of these models assume that the layer growth process is slow and a steady state approximation. Some approximate solutions are also adopted and some property variations (heat conduction resistance, temperature of the crystal layer along the time, and the concentration of feed along the crystallizer, etc.) are neglected to obtain simpler equations. It is clear that steady layer growth requires steady and ideal thermal field in these models, which demand the precise operation profiles. The key operational parameters should be outlined.

According to the reported work,^{1,50,54–56} the following operation parameters that had significant impact on the crystal layer growth were proposed: the initial feed concentration, the feed rate, and the cooling rate. Because the initial feed condition is commonly limited by the upstream condition, the latter two parameters are the key operational parameters in industrial simulation and design.

The models listed in Table 2 can simulate layer thickness distributions of the crystal layer along the crystallizer and predict the temperature distribution along the axial and radial directions. As shown in Figure 9, simulative results from an experimental scale to industrial scale of the overall layer growth

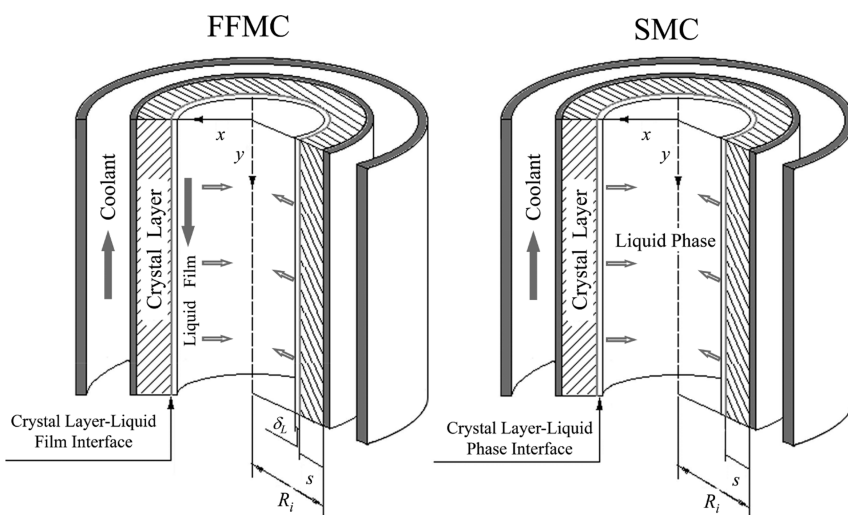


Figure 8. Model configuration of falling film melt crystallization (FFMC). Reproduced with permission from ref 53. Copyright 2014 Elsevier.

Table 2. Model of Crystal Layer Growth in Layer Melt Crystallization

Process type	Principal Model Equation	Model Assumption	Ref.
	$\frac{ds}{dt} = -\frac{\alpha_l(T_b - T_m)}{\rho\lambda'} + \frac{k_{cl}}{\rho\lambda'(R_i + s)} \frac{T_m - T(R_i)}{\ln(R_i + s) - \ln(R_i)} \quad (1)$	(a) a quasi-steady-state model; (b) the layer stops to grow or grows very slowly.	26
	$\frac{\partial G}{\partial X} = \frac{1}{4(\beta + X)^2} \left[(1 - 2\beta + 2\beta^2)(1 - e^{2X}) + 2(1 - 2\beta)Xe^{2X} - 2X^2e^{2X} \right] \quad (2)$ where $X = \ln\left(\frac{R(t)}{R_i}\right); \beta = \frac{k}{hR_i}$.	(a) the substances properties are homogeneous within the range of process conditions; (b) the temperature variation of crystal layer along the crystallization time is neglectable. (c) the layer thickness increases monotonically with the time; (d) the second-order approximate solution.	29
Static melt crystallization (layer growth on the outer cold surface)	$\frac{ds}{dt} = -\frac{\alpha_l(T_b - T_m)}{\rho\lambda'} + \frac{k_{cl}}{\rho\lambda'[R_i + s]} \times \left\{ R_i \left(\frac{\partial T_s}{\partial R} \right)_{R=R_i} + \frac{d}{dt} \left[\int_{R_i}^{R_{i+s}} (T_s(R, t) - T_m) R dR \right] \right\} \quad (3)$ $\alpha_c(t)[T_m(t) - T_{eq}(t)] + \rho_c \lambda'(t) G = k_c \left[\frac{\partial T_c(t)}{\partial R} \right]_{R_{i+s}} \quad (4)$ Where $\lambda' = \lambda_{q,i}^{SL} + C_{p,m}(t)[T_m(t) - T_{eq}(t)]$ $T_{cr}(t) = a(t)(R - R_i)^2 + b(t)(R - R_i) + c(t).$	(a) a site specific heat flow balance at the moving boundary layer; (b) one-dimensional, unsteady, Fourier- differential equation for a cylinder. (a) a steady state, the temperature of the melt is changing negligibly slow. (b) no radial temperature profile in the melt. (c) crystal layer surface is smooth and two-dimensional.	30 57
	$G = G_0 + \frac{k_{cl}v_{co}(k_{cl}v_{co} - j_1G_0)}{2R_i\lambda\rho_c(3k_{cl}v_{co} - j_1G_0)} t \quad (5)$ Where $G_0 = \left(\sqrt{j_i^2 + 4\lambda\rho_c k_{cl} v_{co}} - j_i \right) / (2\lambda\rho_c)$, $j_1 = \Delta T_i = (T_{c-i0} - T_0) \exp\left(-\frac{\alpha_l}{2\pi C_{p,l}\rho_l}\right).$	(a) The cooling temperature along the axial direction of the crystallizer remains constant. (b) The mass and heat transfer along the axial direction of the crystallizer are negligible. (c) The liquid phase is an incompressible fluid.	53
Dynamic melt crystallization (layer growth on the inner cold surface)	$G = \left(\frac{1}{k_o} + \frac{1}{k_i} \right)^{-1} \times \frac{C_o - C_{eq}}{\rho_c} \quad (6)$ $C_b(y) = \left(\int_0^y \frac{-K(y)C_{eq}(y)}{\bar{u}} \exp\left(-\frac{\int_0^y K(y)dy}{\bar{u}}\right) dy + C_0 \right) \exp\left(\frac{\int_0^y K(y)dy}{\bar{u}}\right),$ $K = -\left(\frac{1}{k_o} + \frac{1}{k_i} \right)^{-1} \times \frac{2R_i}{R_o^2 - R_i^2}.$	(a) constant solute diffusion coefficient, and constant thermal; (b) conductivities and thermal diffusivities of fluid and all solid materials; (c) quasi-steady thickness of crystal layer (quasi-steady boundary); (d) fully developed laminar flow in the annulus; (e) mass and thermal diffusion in the axial direction are negligible. (f) natural convection and radiation effects are negligible.	50
Dynamic melt crystallization (layer growth on the outer cold surface)	$\frac{\partial \theta}{\partial \tau} = \frac{1}{Ste X^2} \left[\frac{\partial^2 \theta}{\partial \xi^2} + \frac{X}{(\beta + \xi X)} \frac{\partial \theta}{\partial \xi} + Ste \xi X \frac{\partial X}{\partial \tau} \frac{\partial \theta}{\partial \xi} \right] \quad (7)$ where $\theta = \frac{T - T_w}{T_i(C_0) - T_w}; Ste = \frac{C_{p,i}[T_i(C_0) - T_w]}{\lambda}$; $\tau = \frac{Ste \alpha_{cr} t}{R_i^2}; \beta = \frac{R_i}{R_o}; X = \frac{s(t)R_i}{R_o}; \xi = \frac{R - R_i}{s(t) - R_i}$. $G = G_0 + \frac{k_{cl}v_{co}(k_{cl}v_{co} - j_1G_0)}{2R_i\lambda\rho_c(3k_{cl}v_{co} - j_1G_0)} t \quad (8)$ where $G_0 = \left(\sqrt{j_i^2 + 4\lambda\rho_c k_{cl} v_{co}} - j_i \right) / (2\lambda\rho_c)$, $j_1 = \Delta T_i = (T_{i0} - T_0) \exp\left(-\frac{L\alpha_l}{C_{p,l}\Gamma}\right).$	(a) the resistance to heat conduction of the tube wall is negligible compared to that of the crystal layer that has solidified; (b) a very small thickness ($X = 0.0001$) of the solid crystal layer was assumed to avoid starting difficulties; (c) the temperature on the surface of falling film is assumed to be the initial temperature of the melt. (a) the thickness of crystal layer is small; (b) the layer grows very slowly; (c) the second-order approximate solution.	28 56

process in FFMC has been reported.⁵⁶ The mathematical model utilized based on eq 5 in Table 2. The simulative results indicate that the crystal layer growth can keep steady and

approximately homogeneous with proper operational profiles (test G, for example). Even under the industrial scale, there are still appropriate operational profiles for certain crystallizers. In

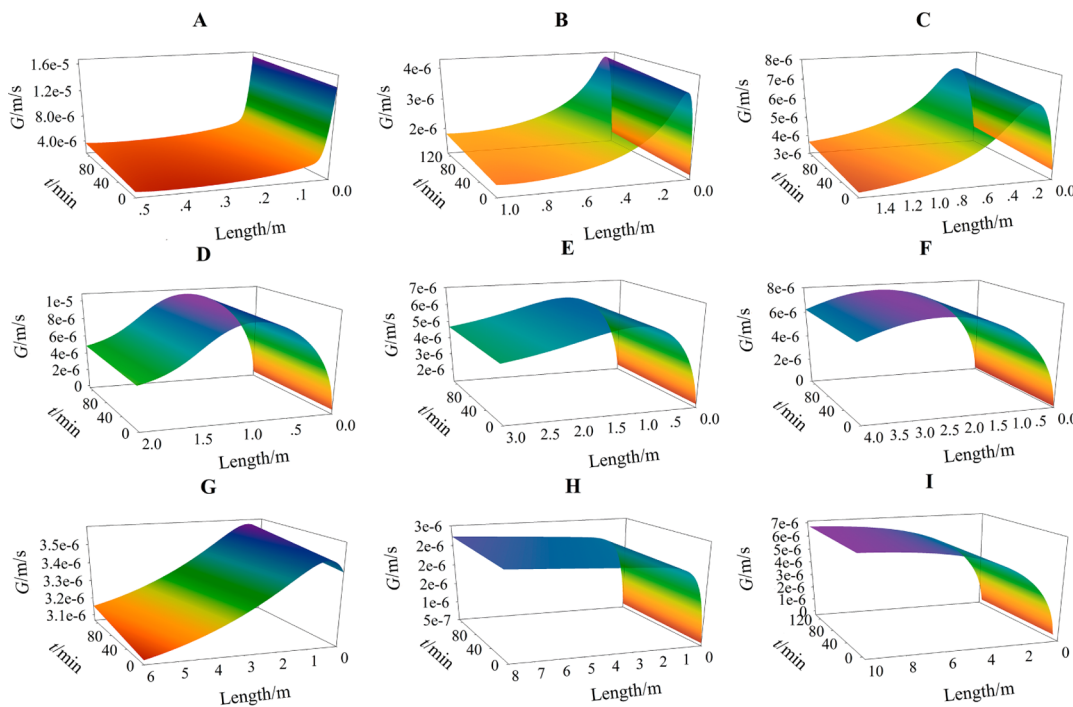


Figure 9. Simulation result of crystal layer growth rate vs time and length in FFMC (the curved surface is semitransparent for a better expression; corresponding operation profiles can be found in ref 56). Reproduced with permission from ref 56. Copyright 2012 Elsevier.

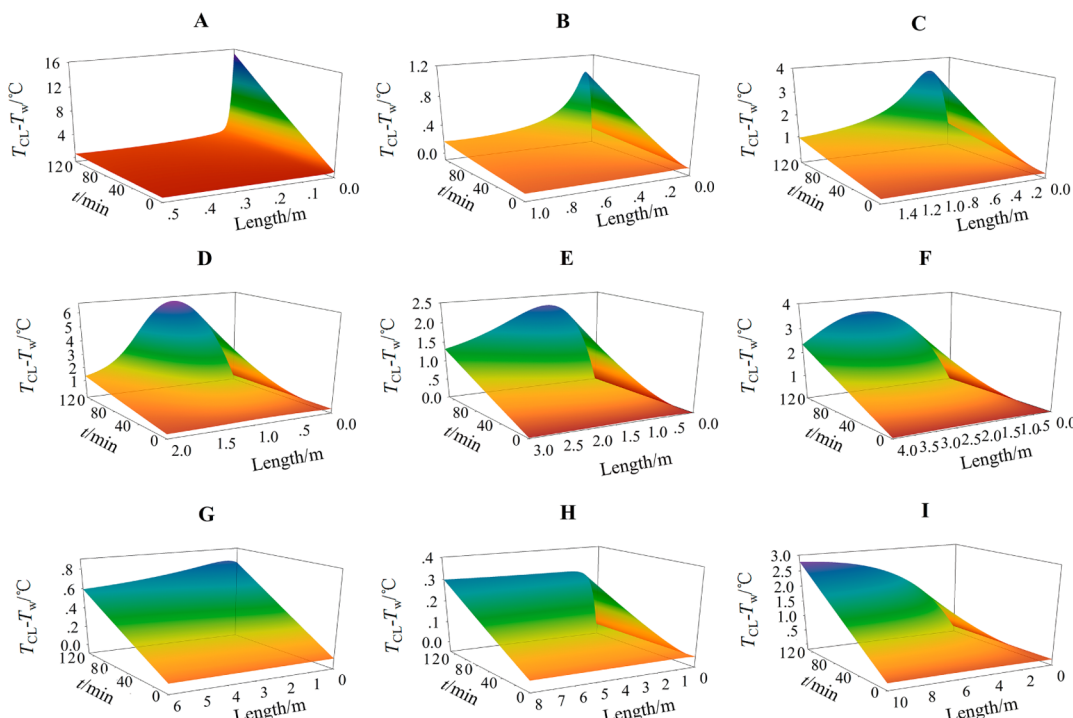


Figure 10. Temperature difference distribution of the crystal layer ($T_{CL} - T_w$) along the crystallizer in FFMC (the curved surface is semitransparent for a better expression; the corresponding operation profiles are the same as the ones in Figure 9).

addition, the feasible dynamic model that meets the actual situation in melt crystallization can reveal the integrated impacts of several key operation conditions on the layer growth and simultaneously, the temperature difference emerges from the crystal layer growth frontier to the cooling wall ($T_{cl} - T_w$) along the crystallizer in FFMC (shown in Figure 10), which are important results to investigate the layer growth and

avoid the partial over quick growth. In the test with steady layer growth (such as test G), the temperature difference distribution along the crystallizer in the overall process is also maintained at a stable state, which is in accordance with the operational cooling curve. With regard to the tests A, B, and C, the crystal layer is in the crisis of over quick growth at the entrance of the crystallizer. The temperature difference sharply increases at the

corresponding location, which results in a very pocket temperature distribution along the axial direction of the crystallizer. The curved surfaces shown in Figure 10 are coincident with the simulation curved surface of layer thickness distribution along the crystallizer in FFMC.⁵⁶ As the main thermal resistance during the layer growth process, the uniform distribution of layer thickness is important for the efficient cooling process. Over quick layer growth and uneconomical cooling can be avoided with the model above. The design cycle and cost are greatly reduced.

3. IMPURITY ENTRAPMENT, MIGRATION, AND DISTRIBUTION IN LAYER MELT CRYSTALLIZATION

The purity of the crystal product and the process of impurity distribution strongly depends on the phase equilibrium and the mass and heat transfer rate at the crystal layer–melt interface. Thus, we introduce the classic theory on the temperature and concentration profiles in layer melt crystallization reported by Kim and Ulrich⁵⁸ before the systematic review on the research of the impurity entrapment, distribution, and migration in melt crystallization.

As shown in Figure 11, the permitted concentration profile can be obtained by utilizing an actual temperature profile and a

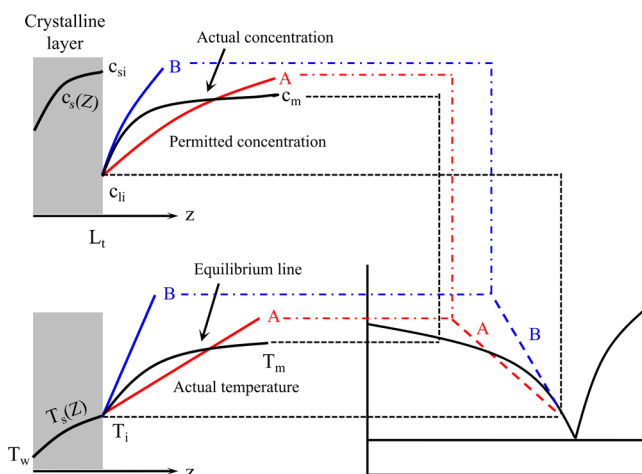


Figure 11. Profiles of temperature and concentration in layer melt crystallization. Reproduced with permission from ref 58. Copyright 2002 Elsevier.

crystal–liquid (c–l) phase diagram. Under the unstable condition (line A), the temperature gradient is large enough for the permitted concentration to be below the actual concentration for all z (along the axial direction of crystallizer), so the liquid phase is always in the single phase region. Under stable condition (line B), the permitted concentration near $z = 0$ is above the actual concentration. The liquid phase is constitutionally supercooled. As discussed above, heterogeneous nucleation is dominant due to extremely high supercooling in the beginning of crystallization. Supercooling means instabilities ahead of the interface may arise. After primary nucleation occurred on the cooling surface, crystal growth becomes the dominant process for the decreasing of the supercooling. As the crystal layer grows by the compound diffusing through the stagnant film of impure melt to a frozen surface where one compound is crystallized, the impure liquid in the equilibrium with the solid at the crystallization temperature is entrapped in the crystal layer.

Eventually, the concentration profile of a component in the crystal layer depends on the initial concentration of the impure melt and the entrapment process of impurities. In the meantime, the location of the c–l interface and profiles of temperature and concentration on both sides of the melt and crystal layer change.

3.1. Model of Impurity Entrapment and Distribution.

The need to simulate the impurity entrapment and illuminate the impact of operating conditions on the separation effect and efficiency has been widely recognized. Abundant literature has been published on this subject.^{51,59,60} It is believed that the impurity entrapment is the synchronization process of crystal layer growth. Thus, impurity entrapment should be simulated as the function of the temperature gradient and system properties. As mentioned, the nucleus activation in melt crystallization is a commonly heterogeneous nucleation process under very high supercooling degree. Thus, the temperature gradient on the layer growth interface will be easily beyond the stable line (line B in Figure 11) and the crystal layer growth rate will increase dramatically. If the temperature gradient exceeds the stable zone (line A in Figure 11), the unbroken crystal layer growth will break down and the growth frontier of the crystal layer tends to form a branched-porous (B–P) structure rather than a smooth one. This B–P surface forms even under the extremely slow cooling process. We propose the B–P criterion to assess the possibility of B–P structure formation in the FFMC process, which is

$$\text{B-P criterion} = \left(\frac{dT_x}{dx} \right)_{x=0} - m \left(\frac{dC_x}{dx} \right)_{x=0} \quad (9)$$

where $m = dT_x^*/dC_l$ is the liquid gradient in the system phase diagram. When the criterion > 0 , there is no B–P structure formed; for the criterion $= 0$, the crystal layer grew at a critical state. When the criterion < 0 , B–P structure occurs: the effective distribution coefficient of impurity should be calculated under the developed model:

Analogous to the differential equation for concentration distribution in a crystal–liquid layer,⁶¹ the impurity balance at the interface can be carried out and the critical temperature gradient ΔT_{cr} is expressed as

$$\Delta T_{cr} = \frac{\delta_l m G C_{0,im}}{D_{im}[K_{id}/(1 - K_{id}) + \exp(-G\delta_D/D_{im})]} \quad (10)$$

where δ_l is the thickness of liquid film and $\delta_{D,i}$ is the thickness of the impurity transfer on the crystal–liquid interface. The critical length L_{cr} should be expressed as

$$L_{cr} = -\frac{\Gamma C_{p,l}}{\alpha_l} \ln \left(\frac{\delta_l m G C_{0,im}}{(T_{i0} - T_0) D_{im}[K_{id}/(1 - K_{id}) + \exp(-G\delta_D/D_{im})]} \right) \quad (11)$$

The developed model to calculate K_{eff} is listed in Table 3 with other reported models (the nomenclature of each model had been unified for a clear expression). With the knowledge of basic phase equilibrium and physical data, measuring ideal distribution coefficient K_{id} and diffusion coefficient δ_D/D_{im} are challenging. As reported in ref 51, a gradient freeze technology (the experimental setup is shown in Figure 7) has been implemented to simulate the ideal impurity distribution process on the crystal–liquid interface during the layer crystallization. The measured data meet the proposed model with good agreement.

Table 3. Effective Distribution Coefficient K_{eff} of Impurity in Layer Melt Crystallization

Process type	Principal Model Equations	Ref.
	$K_{\text{eff}} = \frac{C_{c,i,m}}{C_{b,i,m}} = 1 - \frac{C_{l,\text{int}} - C_{b,i,m}}{C_{b,i,m} \left[\exp\left(\frac{G\rho_{cl}}{D\rho_l}\right) - 1 \right]} \quad (12)$	55
	$K_{\text{eff}} = \frac{C_f - C_{fi}}{1 - C_{fi}} \quad (13),$	47
	where $C_{fi} = aT_0 + b$, a and b are variables related to the separation system.	
SMC	$K_{\text{eff}} = \frac{C_{cl,\text{int}}}{C_{b,i,m}} = \frac{\exp V - (C_{l,\text{int}}/C_{b,i,m})}{\exp V - 1} \quad (14),$	62
	where $V = G\delta_D/D_{im}$.	
	$K_{\text{eff}} = \frac{C_{c,i,m}}{C_{m,i,m}} = 1 - \frac{\Delta c/\Delta c_{\max}}{\frac{C_{m,i,m}}{\left[\exp\left(\frac{G\rho_c}{D_{im}\rho_l}\right) - 1 \right]}} \quad (15)$	63
FFMC(no structure)	B-P $K_{\text{eff}} = \frac{K_{id}}{K_{id} + (1 - K_{id}) \exp(-G\delta_D/D_{im})} \quad (16)$	56
FFMC(with structure)	B-P $K'_{\text{eff}} = 1 - \frac{D\Delta T_l}{\delta_l m G C_{0,im} \exp(-G\delta_D/D_{im})} \quad (17)$	56

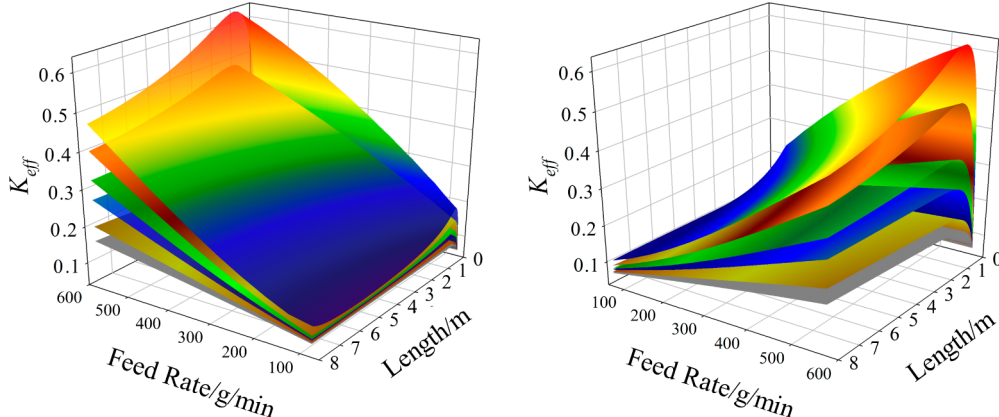


Figure 12. Simulation results of key operational conditions vs $K_{\text{eff},\text{Ca}}$. (The left figure is the front view, and the right figure is the back view. The cooling rate of each surface (from the top to the bottom): rainbow, 0.05 K/min; brown, 0.033 K/min; green, 0.02 K/min; blue, 0.0133 K/min; straw-color, 0.0067 K/min; gray, 0.004 K/min.) Data taken from ref 56.

Note that ΔT_{cr} and L_{cr} are two critical parameters in FFMC process operation and design with known K_{id} and $\delta_{D,i}/D_i$. In the FFMC process, the linear sprinkle density Γ clearly becomes an additional impact that leads to the variations of layer growth rate G , critical length L_{cr} and overall effective distribution coefficient K_{eff} compared to SMC.

According to eq 10, 15 and 16, as the crystal layer composed by partly B-P structure and partly no B-P structure, the simplified expression of \bar{K}_{eff} is

$$\bar{K}_{\text{eff}} = K_{\text{eff}} \frac{L_{\text{cr}}}{L} + K'_{\text{eff}} \left(1 - \frac{L_{\text{cr}}}{L} \right) \quad (18)$$

Thus, the impurity entrapped in the B-P structure and distributed through the porous channels along the crystal layer is in accordance with the crystal layer growth rate distribution. Equation 18 means that the fast and breakage frontier of layer growth tends to entrap more impurity phase than the slow and undercontrolled layer growth frontier. This conclusion has been

verified by the experimental and simulative results in refs 56 and 59 with good agreement.

Moreover, the developing model on the impurity distribution in FFMC is contributing to simulate the effect of various operational parameters on K_{eff} . The impact of the key operational conditions (cooling rate, initial temperature gradient, feed date, and the length of the crystal tower) on the impurity ion (Ca^{2+}) distribution in FFMC is simulated based on the model of impurity distribution, and the simulative results are shown in Figures 12 and 13. (The basic physical and chemical property data are taken from refs 51 and 64.). In Figure 12, the initial temperature gradient (1.08 K) in the FFMC process and the compound of raw material are constant in each simulative test. The surface of $K_{\text{eff},\text{Ca}}$ is diverse along the length of the crystallizer (from the top to the bottom of the crystal tower). It is clearly demonstrated that when the cooling rate is high (the rainbow colored surface in Figure 12), the proportion of impurities entrapped in the crystal layer is also high because of the uncontrolled crystal layer growth and impurity distribution process. The unsatisfactory distribution

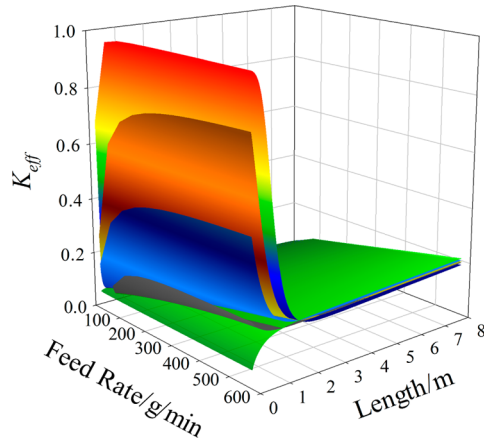


Figure 13. Simulation results of key operational conditions vs $K_{\text{eff},\text{Ca}}$. (The initial temperature gradient $\Delta T_{l,0}$ of each surface (from top to bottom): rainbow, -6.12 K ; brown, -3.12 K ; blue, -1.62 K ; gray, -0.62 K ; green, 0.08 K . Data taken from ref 56.

reaches its peak at a certain position along the crystal tower. The entrapment of impurities then begins to ease with the decrease of the crystal layer growth rate. Note that this ease of impurities entrapment comes at the expense of crystal product yield: the compound concentration of the mother liquid declines very fast because of the uncontrolled layer growth process; as a result, the mother liquid flowing through the majority part of the cooling interface is unsaturated to a grow crystal layer even under a fast cooling curve. At the bottom part of the crystal tower, $K_{\text{eff},\text{Ca}}$ increases in a way due to the breakage of the crystal layer surface and the formation of the B-P structure, the position at the crystal tower is the calculated L_{cr} .

Meanwhile, the feed rate, which is directly proportional to Γ , has presented a distinct influence on the impurities distribution under the same cooling rate. This is because the excess mother liquid will form one excessively thick liquid film which can crash the steady layer growth frontier. In addition, when the feed rate is beyond the upper limit of the crystal tower's cooling capacity, the overheated liquid film is harmful to the porous crystal layer frontier due to the accelerating of impurity absorption and diffusion in the pores of the crystal layer. Note that in the simulative system, when the cooling rate is slower than $0.0133\text{ K}/\text{min}$ (the blue surface in Figure 12), $K_{\text{eff},\text{Ca}}$ gets stable around $0.1\text{--}0.2$, which is satisfactory in a one-stage operation considering the initial concentration of impurity ($2\text{--}3\text{ ppm}$).

Moreover, the impact of the initial temperature gradient on the FFMC process can be simulated with the mentioned theory and developing model. The results are shown in Figure 13. The cooling rate ($0.0133\text{ K}/\text{min}$) in the FFMC process and the compound of raw material are the same in each simulative test. It is indicated that the impurity distribution process is very sensitive to the initial temperature gradient: if the feed material is supercooled, the impure compound will easily be entrapped in the porous crystal layer even if the cooling rate is appropriate. Note that when the initial temperature gradient is -6.12 K (the rainbow colored surface in Figure 13), $K_{\text{eff},\text{Ca}}$ is up to 0.9 at the top part of the crystal tower, which means there is hardly any separation effect; when the initial temperature gradient is -1.62 K (the blue surface in Figure 13), $K_{\text{eff},\text{Ca}}$ decreases to around 0.4 . In addition, the impact of feed rate on

impurity entrapment is very sensitive to the initial temperature gradient: $K_{\text{eff},\text{Ca}}$ increases significantly with the increase of feed rate. Impurity entrapment gets worse when the supercooling degree becomes greater. The key difference between the supercooled ($\Delta T_{l,0} < 0$) feed and overheated ($\Delta T_{l,0} > 0$) feed simulative tests is how $K_{\text{eff},\text{Ca}}$ varies at the top of the crystal tower in the test, which means the temperature control of the feed material should be the principal concerns of the research. Simulation results also show that under overheated ($\Delta T_{l,0} > 0$) feed condition, the increase of the overheating degree will not lead to a better separation effect; the average K_{eff} decreases from 0.064 to 0.058 when $\Delta T_{l,0}$ increases from 0.08 to 3.12 K , for example.

Therefore, model development of the impurity entrapment, distribution process is a very meaningful work for the evaluation and determination of layer melt crystallization operation profiles. The simulative results of the impurity entrapment, distribution processes are also the design basis of the subsequent sweating process.

The preceding model is based on the assumption that the impurity concentration is small and the diffusion layer is very thin. The established dynamic melt crystallization equipment in the laboratory and industrial plants should be well-designed to keep the feed material well-dispersed in the crystallizer. Moreover, the preferable feed material is the preprocessed or purified one to diminish the concentration polarization and diffusion difficulty caused by the high impurity concentration.

In summary, the preferable application field of layer melt crystallization is essentially limited by impurity entrapment and the distribution process in the crystal layer. To fully exhibit the separation potentials of the layer melt crystallization, the feed material should be sufficiently pure. The proper feed is helpful to prepare the ultrapure product with high efficiency. Of course, with assistance of the developing process model on impurity entrapment and distribution, the limitation of feed material purity of layer melt crystallization will be partly weakened.

3.2. Model of the Sweating Process and Impurity Migration

Migration. In general, liquid impurity in the crystal layer is removed by sweating or washing. It is apparent that the purification mechanism differs depending on the state of the impurity. A schematic illustration of impurity purification is shown in Figure 14. The impurities can be entrapped in

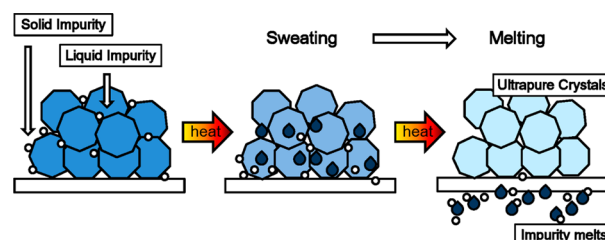


Figure 14. Schematic illustration of impurity purification in the sweating process.

different parts: adhering the melt, liquid phase in the porous channels formed by crystals, liquid phase in crystals, and impurities which are distributed throughout the crystal lattice. It has been reported that, except for the impurities distributed throughout the crystal lattice, the other kind of liquid impurity entrapped can be migrated during the sweating process.^{41–43,59} Moreover, solid impurity is also removed by transferring with melt flow. The sweating process is able to wash the porous

channels in the crystal layer. Thus, sweating is still the most efficient method to remove the impurity and inclusion (especially in the complicated internal porous channels) in the crystal layer of melt crystallization. As illustrated by Ulrich and Kim^{47,59} and König and Schreiner,⁶³ the process control of sweating requires precise operational design of the slight deviation which can lead to an unqualified crystal product with inadequate impurity migration (especially to the impurity entrapped in the close pores and channels of the crystal layer).

The driving force of impurity migration during the sweating process is much more complicated than that of the crystal layer growth process, making the model development on this process quite challenging work. The effect of surface tension gradient (which is created by the heating wall of the crystallizer) on the melt flow is considered to be the critical driving force of liquid impurity migration from the crystal layer.^{64–68} On the other hand, the resistance factor of the sweating process is difficult to generalize because of the complex structure in the crystal layer. Thus, a primary kinetic study on the sweating process should be performed.⁴⁸ Liquid impurity migration is considered an analogical process of liquid entrapment and crystal layer growth. Two main possible resistance factors caused by the structure of the crystal layer are considered: the average tortuosity of porous channels in the crystal layer (τ_{av}) and the porous probability on the crystal layer surface ($P = \phi^{D/3}$). The volume rate of impurity migration can be expressed as

$$G_{sw} = K_{sw} \tau_{av}^a P^b (S_h - 1)^{g_{sw}} \quad (19)$$

where S_h is the superheat degree during the sweating process and a , b , and g_{sw} are the orders of every parameter, respectively. The structural kinetic models of the sweating process in SMC and FFMC fitted with the experimental results are listed in Table 4. The conventional model without considering structural parameters as the resistance factor is listed in the table as a comparison.

Table 4. Models of the Sweating Process in SMC and FFMC⁴⁸

Model type	Equation	R^2
conventional model	$G_{sw, SMC} = 3.576(S_h - 1)^{0.698}$	0.948
	$G_{sw, FFMC} = 2.509(S_h - 1)^{0.724}$	0.958
structural model in Ref. 44	$G_{sw, SMC} = 0.703\tau_{av}^{-3.917}P^{-1.230}(S_h - 1)^{0.677}$	0.999
	$G_{sw, FFMC} = 0.717\tau_{av}^{-6.158}P^{-1.319}(S_h - 1)^{0.686}$	1.000

As a semiempirical model, eq 21 and 22 obtain a higher fitting accuracy than that of eq 19 and 20. A further interpretation has been proposed:⁴⁸ as the crystal layer grown under different mass transfer process and thermal field, the branched crystal in the layer is formed with different size distribution. In addition, the operation duration of the sweating process is relatively longer than other purification and separation processes (filtration, centrifugation, and washing) even if no branched-porous structure forms in the crystal layer.

Fractal theory and technology have been reported as an effective approach to simulate the seepage process in static melt crystallization, and the developed fractal model has been validated by the optimized separation process.⁶⁷ Jiang et al.⁴⁴ considered the sweating process based on analogies with the simulated seepage process: the temperature gradient on the crystal layer is the main driving force of impurity migration, and

the conventional function of seepage process reported by Yu and Cheng⁶⁸ can be developed as follows:

$$q(t, \lambda) = \frac{\pi \Delta P(t) \lambda^4}{128 \mu L_{x-y}} \quad (24)$$

where $q(t, \lambda)$ is the flow rate of impurity liquid migration, L_{x-y} is the overall length of the porous channel length for sweating liquid migration, $\Delta P(t)$ is the pressure difference, and t is the sweating duration. As mentioned above, the surface tension σ is the main driving force of the sweating process, which is fitted by the temperature with an approximate linear equation: $\sigma = c - bT$, where b and c are the constants depending on the system and T is the liquid phase temperature. Thus, the pressure difference $\Delta P(t)$ is expressed as follows:

$$\Delta P(t) = \frac{2\Delta\sigma}{R} = \frac{4b\Delta T(t)}{\lambda} \quad (25)$$

where R is the radius of the pore channel and $\Delta T(t)$ is the temperature difference of the liquid filled in the porous channels. Assuming that the temperature gradient is uniform in the thin enough crystal layer, there is

$$\Delta T(t) = v_{sw} t \left(\frac{l(t)}{l_0} \right) \quad (26)$$

where v_{sw} is the heating rate during the nonisothermal sweating process; $l(t)$ is the length of the liquid phase in a certain channel at time t , and l_0 is the original length of the liquid phase in the channel. The model with the operation parameters is established. Equations 24 and 25 express how the temperature difference on the crystal layer and heating rate during the sweating process impact the kinetic of impurity liquid migration, which is of great importance in evaluating the separation efficiency of the sweating process. As discussed in section 3.1, $K_{eff,i}$ of the overall process can be simulated, and good agreement had been obtained in the hyperpure phosphoric acid separation experiments reported.⁴⁴ More details on the relevant model development and validations are proposed;⁶⁷ for more information, the reader is referred to the fundamental work on the flow model research in complex unsaturated porous media.^{69–74} Research progress of fractal porous media theory and technology on the relevant process simulation has been overviewed in detail.⁷⁵ Note that when the impurity migrated through the heated crystal layer, the framework of crystal layer becomes melted and fragile. This drawback may reduce the terminal separation efficiency.

Fukui et al. applied melt crystallization to produce high-quality vegetable oil from waste oil based on a relevant phase equilibrium properties study.^{76,77} The high purity of triolein from waste oil was obtained with suitable operation conditions. The distribution coefficient correlated well with the theoretical equation derived on the basis of the “local lever rule” (which was also proposed by Fukui and Maeda⁷⁸) at the interface of the crystal layer and melt. König and Schreiner⁶³ reported from investigations on layer melt crystallization that the distribution and migration of impurities are the function of the operational parameters. They made continual effort to transfer this influence to suspension melt crystallization, which extended the application field of the existing models on impurity distribution and migration.

4. APPLICATIONS OF LAYER MELT CRYSTALLIZATION

4.1. Layer Melt Crystallization in Ultrapure Product Manufacture and Specific Separation Process. It must be pointed out that all the research on the crystal layer growth and impurity distribution processes shares the same goals: optimized separation efficiency of melt crystallization. For now, sweating processes are critical to the ultrapure product preparation and some specific separation processes.

4.1.1. Ultrapure Product Manufacture. The key reason for arousing interest in the application of layer melt crystallization is the increasing demand for ultrapure products manufacture with an energy saving separation technology. Ultrapurification demand (purities up to 99.999 wt % for compounds such as caprolactam and phenol) has been achieved by layer melt crystallization with a cost-efficiency single-crystallization operation and desired separation effect. The separation efficiency of a single-stage operation can be enhanced by a secondary-stage crystallization. (see the additional references list part A in the Supporting Information)

Electrical grade phosphoric acid (usually the sum impurity ion concentration should be less than 1 ppm) can be prepared by either static or dynamic layer melt crystallization.^{79–81} As previously discussed, temperature control along the crystallization in industrial scale is very strict because of the ultrapure separation requirement, which is a challenge not only for the chemical engineering designers but also for the equipment manufacturers.

4.1.2. Water Treatment (Wastewater Recovery, Seawater Distillation, and So Forth). Considering the freezing process is part of the melt crystallization, most water treatment, recovery and ultrapurification processes utilize layer melt crystallization. With two successive layer melt crystallization stages and sufficiently severe operation of the sweating process, the interior of the ice layer would be purified and reached the drinking water standard. Mass loss during the sweating process is also high when the impurity concentration is high. Note that the feasibility of the process still has to be optimized and the cost of the overall process should be evaluated.⁸² As previously mentioned, the dynamic layer melt crystallization is a more attractive technology rather than the static or gradient freezing layer melt crystallization. Thus, the main kinetic parameters influencing the sweating process in dynamic layer melt crystallization are investigated, and a developed statistical model for ice weight and ice purity can optimize the whole desalination process time.²⁵

4.1.3. Specific Separation and Recovery Process in the Nuclear Industry. Uranium recovery from uranyl nitrate hexahydrate (UNH) crystals is still indispensable to the relevant researchers and engineers. As reported by Nakahara et al.,¹² the defined parameters, purification rate coefficients, are sensitive to the sweating temperature (varied from 56 to 57 °C) by the isothermal sweating process. Meanwhile, the separation efficiency varies with the location of the crystal layer because of the different temperatures and impurity distributions, even when the experiments are implemented in laboratorial scale. This conclusion has been verified in separate literature.^{12,44,83} This means the sweating process in melt crystallization requires extremely strict temperature control. To control the temperature with high accuracy, more advanced measurement technology (deviation smaller than 0.1 K, for instance) and novel designed crystallizers are crucial. Meanwhile, with the progress of crystallizer design and crystal layer growth control, a

purer crystal layer with less impurity entrapped will be acquired (the ideal purity can be predicted with the method reported in ref 51). Thus, we are confident to diminish the time and energy consumption of the sweating process step by step. All of the preceding endeavor will be helpful for making melt crystallization a more green and efficient separation technology.

Pyroprocessing, which is one of the promising technologies enabling the recycling of spent nuclear fuels from a commercial light water reactor (LWR), generates a waste LiCl salt containing radioactive elements. Static melt crystallization was presented as the purification process to reuse LiCl salt.⁸⁴ The first-principles calculations and density functional theory that are commonly used as tools to understand the inclusion mechanism of impurities within the LiCl crystal.^{85,86} This impurity inclusion process leading to increase of the lattice parameter is a commonly observed phenomenon in experiments.⁸⁷ Based on the first-principles calculations, the high substitution enthalpy results in high impurity separation efficiency, which is consistent with the experimental results. Choi et al.⁸⁴ concluded that the electron density map also gave a clue to the mechanism for inclusion of impurities. Their work also implies that the impurity separation potential of melt crystallization on other fission products such as Eu³⁺ and U³⁺, which is quite important to design with the efficient recycling method of LiCl waste salts during the pyroprocessing.

4.2. Layer Melt Crystallization in Polymeric System. To separate the isomeric long-chain aldehydes, Beierling and Ruether³⁰ conceived layer melt crystallization experiments under an inert gas atmosphere without chemical additives for the separation. Experimental configurations are implemented just like the one utilized in the seawater desalination system.²⁵ A space and time dependent enthalpy balance of the crystal volume and a camera for growth rate measurement are applied. Because of concern that the process conditions (feed concentration and cooling rate) are same with the separation process of inorganic compounds, melt crystallization was utilized, which encourages researchers to apply the existing layer growth and impurity separation models in the polymeric system separation.

Both crystallization and molecular diffusion processes are relatively slow in polymers, the higher order crystalline structure is formed by the competition and interaction between the crystallization and chain diffusion rates, which is hard to simulate with present engineering models in melt crystallization. In the laboratorial scale, the temperature profile of the crystal is assumed to be linear so the layer growth model is simplified. Thus, if applied in industrial scale, more research depth on this model is necessary.

López-Beceiro et al. (see part B of the Supporting Information) provided a model to describe the low-temperature solid phase transformation kinetics. This model fits nicely isothermal and nonisothermal melt crystallization of polymers. The differential scanning calorimetry (DSC) was implemented to observe the preparation process of a metal organic framework (MOF).

Dasgupta et al. found that induction times decreased with low crystallization temperature and the number of nuclei per unit area increased with higher supercooling and cooling rates by investigating the melt crystallization of polyunsaturated fatty acid (PUFA) mixture under various supercooling and cooling rates. For further consideration of the polymeric system, the higher order structure in crystalline–amorphous block copolymers is formed by the combination of the crystallization

and microphase separation (MS) process, which is more complicated than that of melt crystallization of an inorganic system. Thus, the behavior of crystallization in the kinetic aspect should be seriously considered due to the scale-up effect of heat conduction. The research on the mechanism of secondary melt crystallization was proposed by Chen et al. . This mechanism is as complex as they expected and not well understood yet. However, the secondary crystallization undoubtedly increases the melting point of a crystalline polymer by narrowing the distribution crystalline lamellae, and the secondary crystallization rates are limited by the ability of chain entanglements to diffuse away from the growth front and noncrystallizable molecular species as reported. (see the additional references list part B in the Supporting Information)

The kinetics model research on the melt crystallization of a polymeric system relies more on the heat transfer, chemical property, and optical image investigation technologies (DSC, FTIR spectroscopy, polarizing optical microscope (POM), and micro-Fourier transform infrared spectroscopy,⁹¹ etc.) than that of the classical melt crystallization in industrial scale, to some extent (see the additional references list part C in the Supporting Information). In addition, as declared in the latest research on the static layer melt crystallization,⁵⁷ the deviation of crystal thermal conductivity for an experimental uncertainty of 1% of the temperature of the cooling surface is 77.64%. This result raises the requirement on the accurate measurement of the thermal data in layer melt crystallization. These mentioned technologies offer an approach to investigate and simulate the melt crystallization process in laboratorial scale with high accuracy and reliability. Meanwhile, accurate and reliable data are quite helpful to the development and modification of the relevant kinetic model.

4.3. Layer Melt Crystallization in Food Industry. As mentioned in section 2, the nucleation of compounds with ultrasonic technology has the effects of intentional seeding including the shortening of the induction time, narrowing of the metastable zone width, and the control of particle size distribution, which are beneficial in preparing desirable feed slurry and creating a desirable crystallization environment. Additional research on the application of this ultrasonic technology to melt crystallization has received wide attention in the past decade.

Presented reviews of Chandrapala et al.⁸⁸ had summarized selected fields of applications to the food industry (crystallization, freezing, extraction, and thawing, etc.). Ultrasonic method is found to be beneficial in reducing time, in increasing efficiency and yields by controlling the crystal structure and shape, and in the crystallization rate of biological materials. Those who are interested in other possible applications are encouraged to read the excellent extensive review articles of Chandrapala et al. (see the additional references list part D in the Supporting Information) At lower frequencies (20–100 kHz), the physical effects dominate; at intermediate frequencies (200–500 kHz), the number of generated active bubbles is higher and chemical effects are dominant (the highly reactive radicals are formed within the cavitation bubbles).

Rapid sonocrystallization is utilized during the nucleation phase of crystallization for lactose recovery, fat, and proteins in food industries. The application of sonocrystallization in confectionary, vegetable, and milk fats indicates that ultrasound affects crystal size and morphology.^{89,90} Meanwhile, the rapid ultrasound-assisted crystallization application in the recovery of lactose has been investigated. This novel crystallization has the

potential of resolving the main problem of a long induction time and slow crystallization rate because of a large metastable zone width associated with lactose crystallization (see the additional references list part E in the Supporting Information).

An adequate experimental and theory foundation has been established to investigate the ultrasound-assisted crystallization (or sonocrystallization) in the food industry. The research on ultrasound-assisted crystallization is contributing to activating the nucleus and generating the initial crystal layer as reported in the relevant literature.^{91,92} The influence of ultrasound in the layer melt crystallization with gradient freeze technique could be analyzed by numerical simulations with the help of FLUENT. The simulation result demonstrated that ultrasound is contributing to reducing the diffusion boundary layer on the crystal growth frontier effectively.⁹³ The layer melt crystallization with special technology (ultrasonic, gradient freeze, and so forth) is a vivid topic not only for the food industry and industrial separation process.

In addition, the theoretical and experimental approach toward crystallization and liquid phase inclusion processes modeling related to the freezing process had been developed, and the methods to evaluate and monitor the crystallization and ice crystal characteristics during or after freezing were presented.^{94–96} Note that crystal growth and liquid phase distribution study of layer melt crystallization with gradient freeze technology was carried out in various works.^{41–43,58,97,98} This indicates that the food industry and industrial separation share a mutual attention on the layer freezing process though the application areas are diverse from each other.

Food freezing process that involves the phenomenon of water crystallization is complicated. In particular, novel freezing technologies with ultrasound-assisted, high-pressure magnetic resonance have uncovered a positive effect on the nucleation of water crystallization and the control of the crystallization process (see the additional references list part F in the Supporting Information). The theoretical and experimental research results in the crystal layer growth mentioned previously are helpful for improving the freezing process by optimizing the crystal size distribution, crystal location, crystal morphology, and crystal layer structure.⁹⁹ The ultimate goal of any alteration or control of the process is creating fine and numerous crystals, which guarantee a better quality of frozen foods and biomaterials and more desirable initial crystal layer for the coming up layer growth and separation process.¹⁰⁰ In summary, this optimized technology is contributing to obtaining the desired process efficiency and desired quality of the final product, which is the same aim no matter whether it is for the food industry or chemical engineering.

5. PERSPECTIVES AND CONCLUSIONS

To obtain desired ultrapure crystal products in layer melt crystallization, the experimental and model research focus on the key processes which determine the terminal separation efficiency of layer melt crystallization: the crystal layer growth and impurity distribution processes. These two processes are so closely linked that the model development commonly shares the same basic assumption, mass and energy balance theories. The investigation of these two processes is complex and highly interdisciplinary.

The initial crystal layer is of great importance to the desired separation performance during the layer growth process. Heterogeneous nucleation (HEN) is the preferred approach to allow more controllable nucleus growth and to be helpful for

nucleus growth that has a well-behaved initial crystal layer. In addition, the ultrasonic and other physical fields are contributing to reduce the nucleation barrier and keep the nucleation process controllable. As mentioned, the development and modification of the crystal layer growth model are essential to the simulation of the crystal product yield and the operational consumption with high accuracy and stability. Dynamic layer melt crystallization (or FFMC) has obtained our special focus because of the complex operating conditions and their various impacts on the layer growth kinetics. Efforts attempted on the model development to achieve the high-accuracy simulation results have been overviewed, and the various operational profiles and configurations to enhance the desired separation performance are presented. It is believed that the present simulation results have provided important information and guidance for the designers and engineers of industrial crystallization. The proposed assumptions during the model modification have yet to be modified and optimized especially on the simulation at the input and output part of the crystallizer and the crystal layer structure analysis. Moreover, the crystal layer growth determines the impurity distribution and the load of the separation process. The phase transition (crystal phase to melt phase), mass transport (melt through the intricate crystal layer framework, the impurity migration), and heat transport (heat transfer between the cooling surface, crystal and melt, and so forth), are more complex processes than the crystal layer growth.

The application of fractal theory to kinetic analysis of the sweating process is a new concept and yet to be investigated extensively. Preliminary study shows that fractal theory can successfully interrupt the impact of fractal crystal layer structure on the sweating liquid migration. However, implementation and validation in various experimental systems are necessary, which is challenging work requiring more physical and mathematical theory research in depth.

Sweating seems to be the most effective and efficient solution for additional purification in layer melt crystallization from a practical point of view, yet it still suffers from several shortcomings such as the relevant long operation duration, the sharp separation efficiency reduction with excess impurity entrapped in the crystal layer, and the sharp energy and operation cost increasing when the melt point deviation is very small between pure crystal product and impure compound. Coupled processes among various separation technologies should be implemented which calls for wider concerns.

Despite the great potential of the layer melt crystallization, the existing experimental technology and model related theory are still insufficient to fulfill all of the expectations and requirements. Inspiring applications (ultrapure product manufacturer and specific separation process, melt crystallization in polymeric system, and the applications in food industry, etc.) related to layer melt crystallization have been introduced to provide a further insight of this classic and vital separation technology. Advanced thermal and kinetic investigating technologies (FTIR, POM, ultrasound, high pressure, and magnetic resonance, etc.) and strategies are helpful to explore the research perspective of layer melt crystallization. Traditional model expressions used to describe the crystal layer growth and impurity distribution must be modified to account for potential involvement of extra driving force and influence parameters. These applications and technologies are promising for bridging the gap between developments from laboratory research and industry requirements.

Advances toward the process simulation and design in layer melt crystallization have been achieved, while highly stable and tolerant operation profiles for solving the complex large-scale application of layer melt crystallization in wide industrial areas are still unsolved issues. Further research needs to be adequately aligned to the interpretation and kinetic mechanism research of the crystal layer growth and impurity distribution process. Any modifications on the simulative model should involve the operational parameters and provide reliable and stable performance when applied to the practical processes in layer melt crystallization.

■ ASSOCIATED CONTENT

S Supporting Information

Additional references list for the section Applications of Layer Melt Crystallization. This material is available free of charge via the Internet at <http://pubs.acs.org>.

■ AUTHOR INFORMATION

Corresponding Author

*Tel.: +86 411-84707892. Fax: +86 411-84986291. E-mail: xbjiang@dlut.edu.cn.

Notes

The authors declare no competing financial interest.

■ ACKNOWLEDGMENTS

This work is supported by the National Natural Science Foundation of China (Grant Nos. 21306017 and 21206014), the National Science Fund for Distinguished Young Scholars of China (Grant No. 21125628), the China Postdoctoral Science Foundation funded project (Grant No. 2013MS30126), and the Fundamental Research Funds for the Central Universities of China (Grant No. DUT14RC(4)10).

■ NOMENCLATURE

a = variables related to the separation system in eq 12

b = variables related to the separation system in eq 12

C_0 = concentration of the crystallized component at the initial condition

$C_{0,im}$ = mass fractions of impurity i in the feed liquid

C_b = concentration of the crystallized component in bulk liquid

$C_{b,im}$ = impurity concentration in bulk liquid phase

$C_{c,im}$ = concentration of impurities in the crystals

$C_{cl,int}$ = concentration in the crystal layer at the crystal–liquid interface

$C_{cl,im}$ = mass fractions of impurity i in crystal layer

C_{cr} = average concentration in the layer

C_{eq} = concentration of equilibrium liquid phase

C_f = concentration of the crystal layer before sweating

C_{fi} = concentration of inclusions in the crystal layer before sweating

$C_{l,int}$ = concentration in the liquid at the crystal–liquid interface

$C_{p,cl}$ = heat capacity at constant pressure of the crystal layer, $J \text{ kg}^{-1} \text{ K}^{-1}$

$C_{p,l}$ = heat capacity at constant pressure of liquid film, $J \text{ kg}^{-1} \text{ K}^{-1}$

$\Delta c/\Delta c_{\max}$ = concentration increase in the boundary layer

D_{im} = diffusion coefficient of impurity i in liquid film, $\text{m}^2 \text{ s}^{-1}$

G = crystal layer growth rate, m s^{-1}

G_0 = initial crystal layer growth rate, m s^{-1}

j_1 = heat flux of overheat liquid film transferring to the cooling wall, $\text{J m}^{-2} \text{s}^{-1}$
 K_{id} = ideal distribution coefficient of impurity i on the interface
 K_{eff} = effective distribution coefficient of impurity i
 K'_{eff} = effective distribution coefficient of impurity i in B-P crystal layer
 \bar{K}_{eff} = overall effective distribution coefficient of impurity i
 k_{cl} = heat conductivity coefficient of the crystal layer, $\text{W m}^{-1} \text{K}^{-1}$
 L = length of the crystal layer, m
 L_{cr} = critical length, m
 m = liquidus gradient in the system phase diagram, K
 R_i = inner radius of the cooling tube, m
 R_o = outer radius of the cooling tube, m
 s = crystal layer thickness, m
 t = time, s
 T_0 = temperature of liquid film at inlet of crystallizer, K
 T_b = temperature of melt bulk, K
 T_{eq} = equilibrium temperature, K
 T_l = temperature of the liquid film, K
 $T_{l,0}$ = crystal layer–liquid film interface temperature at inlet of crystallizer, K
 T_m = temperature of melting, K
 T_w = temperature of the cooling wall, K
 T_f = temperature before sweating, K
 $T_{c-l,0}$ = temperature of C–L interface at the initial moment, K
 ΔT_l = temperature difference of liquid film, K
 ΔT_{cr} = critical temperature difference, K
 \bar{u} = average velocity, m/s
 v = cooling rate, $^{\circ}\text{C s}^{-1}$
 x = radial position, m
 y = axial position, m

Greek letters

α = heat transfer coefficient, $\text{W m}^{-2} \text{K}^{-1}$
 δ_D = thickness of mass transfer boundary layer, m
 δ_l = thickness of liquid film, m
 θ = dimensionless temperature
 λ = crystallization latent heat, J kg^{-1}
 λ_{0i}^{SL} = heat of fusion of crystallizing component, J kg^{-1}
 λ' = sum of the heat released by the crystallization, J
 Γ = linear spray density, $\text{kg m}^{-1} \text{s}^{-1}$
 ξ = transformed radial coordinate
 ρ_c = density of the crystal phase, kg m^{-3}
 ρ_{cl} = density of the crystal layer, kg m^{-3}
 ρ_l = density of the liquid phase, kg m^{-3}

Subscripts

0 = initial condition
 b = Bulk of melt (liquid) phase
 c = crystal
 cl = crystal layer
 co = cooling
 cr = critical
 eq = equilibrium
 i = inner side
 im = impurity
 int = interface
 l = liquid
 m = melt
 o = outer side
 w = wall

■ REFERENCES

- (1) Ulrich, J. Is melt crystallization a green technology? *Cryst. Growth Des.* **2004**, *4* (5), 879–880.
- (2) Ulrich, J.; Biilau, H. C. In *Melt Crystallization in Handbook of Industrial Crystallization*, Vol. 7; Myerson, A. S., Ed.; Butterworth-Heinemann: Boston, MA, USA, 2002.
- (3) Wintermantel, K.; Wellinghoff, G. In *Layer Crystallization and Melt Solidification in Crystallization Technology Handbook*, Vol. 14; Mersmann, A., Ed.; Dekker: New York, 2001.
- (4) Kashchiev, D. *Nucleation: Basic Theory with Applications*; Butterworth-Heinemann: Oxford, U.K., 2000.
- (5) Jung, J. W.; Lee, H. S.; Kim, K.-J. Purification of Acetic Acid Wastewater using Layer Melt Crystallization. *Sep. Sci. Technol.* **2008**, *43* (5), 1021–1033.
- (6) König, A.; Stepanki, M.; Kuszlik, A.; Keil, P.; Weller, C. Ultra-purification of ionic liquids by melt crystallization. *Chem. Eng. Res. Des.* **2008**, *86* (7), 775–780.
- (7) Luo, C.-s.; Chen, W.-w.; Han, W.-f. Experimental study on factors affecting the quality of ice crystal during the freezing concentration for the brackish water. *Desalination* **2010**, *260* (1), 231–238.
- (8) Marion, G.; Farren, R.; Komrowski, A. Alternative pathways for seawater freezing. *Cold Reg. Sci. Technol.* **1999**, *29* (3), 259–266.
- (9) Rodriguez, M.; Luque, S.; Alvarez, J.; Coca, J. A comparative study of reverse osmosis and freeze concentration for the removal of valeric acid from wastewaters. *Desalination* **2000**, *127* (1), 1–11.
- (10) Wakisaka, M.; Shirai, Y.; Sakashita, S. Ice crystallization in a pilot-scale freeze wastewater treatment system. *Chem. Eng. Process.* **2001**, *40* (3), 201–208.
- (11) Nakahara, M.; Koizumi, T.; Nomura, K. Enhancement of Decontamination Performance of Impurities for Uranyl Nitrate Hexahydrate Crystalline Particles by Crystal Purification Operation. *Nucl. Technol.* **2011**, *174* (1), 77–84.
- (12) Nakahara, M.; Nomura, K.; Koizumi, T. Purification Rate of Uranyl Nitrate Hexahydrate Crystal for Transuranium Elements on Isothermal Sweating Phenomenon. *Ind. Eng. Chem. Res.* **2010**, *49* (22), 11661–11666.
- (13) Nakahara, M.; Nomura, K.; Washiya, T.; Chikazawa, T.; Hirayama, I. Removal of Liquid and Solid Impurities from Uranyl Nitrate Hexahydrate Crystalline Particles in Crystal Purification Process. *J. Nucl. Sci. Technol.* **2011**, *48* (3), 322–329.
- (14) Inada, T.; Zhang, X.; Yabe, A.; Kozawa, Y. Active control of phase change from supercooled water to ice by ultrasonic vibration 1. Control of freezing temperature. *Int. J. Heat Mass Transfer* **2001**, *44* (23), 4523–4531.
- (15) Nakagawa, K.; Hottot, A.; Vessot, S.; Andrieu, J. Influence of controlled nucleation by ultrasounds on ice morphology of frozen formulations for pharmaceutical proteins freeze-drying. *Chem. Eng. Process.* **2006**, *45* (9), 783–791.
- (16) Fuchigami, M.; Teramoto, A. Structural and Textural Changes in Kinu-Tofu Due to High-Pressure-Freezing. *J. Food Sci.* **1997**, *62* (4), 828–837.
- (17) Micovic, J.; Beierling, T.; Lutze, P.; Sadowski, G.; Góral, A. Design of hybrid distillation/melt crystallisation processes for separation of close boiling mixtures. *Chem. Eng. Process.* **2013**, *67*, 16–24.
- (18) Martini, S.; Suzuki, A.; Hartel, R. Effect of high intensity ultrasound on crystallization behavior of anhydrous milk fat. *J. Am. Oil Chem. Soc.* **2008**, *85* (7), 621–628.
- (19) Wagterveld, R. M.; Miedema, H.; Witkamp, G.-J. Effect of ultrasonic treatment on early growth during CaCO_3 precipitation. *Cryst. Growth Des.* **2012**, *12* (9), 4403–4410.
- (20) Chianese, A.; Cipriani, P.; Parisi, M. Purification of ϵ -caprolactam by means of a new dry-sweating technique. *Chem. Eng. J.* **2002**, *87* (2), 187–195.
- (21) Mandri, Y.; Rich, A.; Mangin, D.; Abderafi, S.; Bebon, C.; Semlali, N.; Klein, J.-P.; Bounahmidi, T.; Bouhaouss, A. Parametric study of the sweating step in the seawater desalination process by indirect freezing. *Desalination* **2011**, *269* (1–3), 142–147.

- (22) Tavare, N. *Industrial Crystallization—Process Simulation Analysis and Design*; Plenum: New York, 1995.
- (23) Henning, S.; Ulrich, J. Description of the Migration of Liquid Inclusions in Growing Crystalline Layers. *Chem. Eng. Res. Des.* **1997**, *75* (2), 233–236.
- (24) Ramkrishna, D. *Population Balances: Theory and Applications to Particulate Systems in Engineering*. Academic Press: San Diego, CA, USA, 2000.
- (25) Rich, A.; Mandri, Y.; Mangin, D.; Rivoire, A.; Abderafi, S.; Bebon, C.; Semlali, N.; Klein, J.-P.; Bounahmidi, T.; Bouhaouss, A.; Veesler, S. Sea water desalination by dynamic layer melt crystallization: Parametric study of the freezing and sweating steps. *J. Cryst. Growth* **2012**, *342* (1), 110–116.
- (26) Chianese, A.; Santilli, N. Modelling of the solid layer growth from melt crystallization—The integral formulation approach. *Chem. Eng. Sci.* **1998**, *53* (1), 107–111.
- (27) Briançon, S.; Colson, D.; Klein, J. Modelling of crystalline layer growth using kinetic data obtained from suspension crystallization. *Chem. Eng. J.* **1998**, *70* (1), 55–64.
- (28) Radhakrishnan, K.; Balakrishnan, A. Kinetics of melt crystallization in falling films. *Chem. Eng. Commun.* **1999**, *171* (1), 29–53.
- (29) Guardani, R.; Neiro, S.; Büla, H.; Ulrich, J. Experimental comparison and simulation of static and dynamic solid layer melt crystallization. *Chem. Eng. Sci.* **2001**, *56* (7), 2371–2379.
- (30) Beierling, T.; Ruether, F. Separation of the isomeric long-chain aldehydes dodecanal/2-methylundecanal via layer melt crystallization. *Chem. Eng. Sci.* **2012**, *77*, 71–77.
- (31) Choi, W. S.; Kim, K.-J. Separation of Acetic Acid from Acetic Acid-Water Mixture by Crystallization. *Sep. Sci. Technol.* **2013**, *48* (7), 1056–1061.
- (32) Kim, K. J. Purification of phosphoric acid from waste acid etchant using layer melt crystallization. *Chem. Eng. Technol.* **2006**, *29* (2), 271–276.
- (33) Wang, B.; Li, J.; Qi, Y.; Jia, X.; Luo, J. Phosphoric acid purification by suspension melt crystallization: Parametric study of the crystallization and sweating steps. *Cryst. Res. Technol.* **2012**, *47* (10), 1113–1120.
- (34) Kashchiev, D.; van Rosmalen, G. Review: Nucleation in solutions revisited. *Cryst. Res. Technol.* **2003**, *38* (7–8), 555–574.
- (35) Mullin, J. W. *Crystallization*; Butterworth-Heinemann: Oxford, U.K., 1993.
- (36) Haasner, T.; Kuszlik, A. K.; Stadler, R.; Ulrich, J. Surface Properties—A Key for Nucleation in Melt Crystallization Processes. *Chem. Eng. Technol.* **2001**, *24*, 873–878.
- (37) Dang, L.; Wei, H.; Wang, J. Effects of ionic impurities (Fe^{2+} and SO_4^{2-}) on the crystal growth and morphology of phosphoric acid hemihydrate during batch crystallization. *Ind. Eng. Chem. Res.* **2007**, *46* (10), 3341–3347.
- (38) Dang, L.; Wang, Z.; Liu, P. Measurement of the metastable zone width of phosphoric acid hemihydrate in the presence of impurity ions. *J. Chem. Eng. Data* **2007**, *52* (5), 1545–1547.
- (39) Narducci, O.; Jones, A.; Kougooulos, E. An assessment of the use of ultrasound in the particle engineering of micrometer-scale adipic acid crystals. *Cryst. Growth Des.* **2011**, *11* (5), 1742–1749.
- (40) Narducci, O.; Jones, A.; Kougooulos, E. Continuous crystallization of adipic acid with ultrasound. *Chem. Eng. Sci.* **2011**, *66* (6), 1069–1076.
- (41) Narducci, O.; Jones, A.; Kougooulos, E. Crystal product engineering in the seeded cooling crystallization of adipic acid from aqueous solution. *Org. Process Res. Dev.* **2011**, *15* (5), 974–980.
- (42) Narducci, O.; Jones, A. Seeding in Situ the Cooling Crystallization of Adipic Acid using Ultrasound. *Cryst. Growth Des.* **2012**, *12* (4), 1727–1735.
- (43) Scholz, R.; Wangnick, K.; Ulrich, J. On the distribution and movement of impurities in crystalline layers in melt crystallization processes. *J. Phys. D: Appl. Phys.* **1993**, *26* (8B), B156.
- (44) Jiang, X.; Hou, B.; He, G.; Wang, J. Falling film melt crystallization (II): Model to simulate the dynamic sweating using fractal porous media theory. *Chem. Eng. Sci.* **2013**, *91*, 111–121.
- (45) Kim, K.-J.; Ulrich, J. Theoretical and experimental studies on the behaviour of liquid impurity in solid layer melt crystallizations. *J. Phys. D: Appl. Phys.* **2001**, *34* (9), 1308.
- (46) Parisi, M.; Chianese, A. The crystal layer growth from a well-mixed melt. *Chem. Eng. Sci.* **2001**, *56* (14), 4245–4256.
- (47) Kim, K.-J.; Ulrich, J. A quantitative estimation of purity and yield of crystalline layers concerning sweating operations. *J. Cryst. Growth* **2002**, *234* (2), 551–560.
- (48) Jiang, X.; Hou, B.; Zhao, Y.; Wang, J.; Zhang, M. Kinetics Study on the Liquid Entrapment and Melt Transport of Static and Falling-Film Melt Crystallization. *Ind. Eng. Chem. Res.* **2012**, *51* (13), 5037–5044.
- (49) Cong, S.; Li, X.; Wu, J.; Xu, C. Optimization of Parameters for Melt Crystallization of p-Cresol. *Chin. J. Chem. Eng.* **2012**, *20* (4), 649–653.
- (50) Zhou, L.; Su, M.; Benyahia, B.; Singh, A.; Barton, P. I.; Trout, B. L.; Myerson, A. S.; Braatz, R. D. Mathematical modeling and design of layer crystallization in a concentric annulus with and without recirculation. *AIChE J.* **2013**, *59* (4), 1308–1321.
- (51) Jiang, X.; Wang, J.; Hou, B. Coarse crystal layer growth and liquid entrapment study with gradient freeze technology. *Cryst. Res. Technol.* **2012**, *47* (6), 649–657.
- (52) Rubbo, M. Basic concepts in crystal growth. *Cryst. Res. Technol.* **2013**, *48* (10), 676–705.
- (53) Jiang, X.; Xiao, W.; He, G. Falling film melt crystallization (III): Model development, separation effect compared to static melt crystallization and process optimization. *Chem. Eng. Sci.* **2014**, *117*, 198–209.
- (54) Mersmann, A. *Crystallization Technology Handbook*, 2nd ed.; Dekker: New York, 2001.
- (55) Myerson, A. S. *Handbook of Industrial Crystallization*, 2nd ed.; Butterworth-Heinemann: Boston, MA, USA, 2002.
- (56) Jiang, X.; Hou, B.; He, G.; Wang, J. Falling film melt crystallization (I): Model development, experimental validation of crystal layer growth and impurity distribution process. *Chem. Eng. Sci.* **2012**, *84*, 120–133.
- (57) Beierling, T.; Gorny, R.; Sadowski, G. Modeling Growth Rates in Static Layer Melt Crystallization. *Cryst. Growth Des.* **2013**, *13* (12), 5229–5240.
- (58) Kim, K.-J.; Ulrich, J. Impurity Distribution in a Solid–Liquid Interface during Static Layer Crystallization. *J. Colloid Interface Sci.* **2002**, *252* (1), 161–168.
- (59) Kim, K.-J.; Ulrich, J. Purification of crystalline layers by controlling the temperature gradient. *Powder Technol.* **2001**, *121* (1), 81–87.
- (60) Myasnikov, S. Transport of impurities out of a two-phase crystal layer into a melt under the effect of a temperature gradient: Mechanisms and kinetics. *Theor. Found. Chem. Eng.* **2003**, *37* (2), 137–143.
- (61) Arkenbout, G. F. *Melt crystallization technology*; Technomic: Lancaster, PA, USA, 1995.
- (62) Myasnikov, S.; Uteshinsky, A. Melt entrapment during growth of crystal layer with nonplanar interface and diffusive transport of captured impurities out of layer pores. *J. Cryst. Growth* **2005**, *275* (1), e39–e45.
- (63) König, A.; Schreiner, A. Purification potential of melt crystallisation. *Powder Technol.* **2001**, *121* (1), 88–92.
- (64) Voorhees, P.; Coriell, S.; McFadden, G.; Sekerka, R. The effect of anisotropic crystal-melt surface tension on grain boundary groove morphology. *J. Cryst. Growth* **1984**, *67* (3), 425–440.
- (65) Schwabe, D. Surface-tension-driven flow in crystal growth melts. In *Superhard Materials, Convection, and Optical Devices*; Springer: Berlin, 1988; pp 75–112.
- (66) Leypoldt, J.; Kuhlmann, H. C.; Rath, H. J. Three-dimensional numerical simulation of thermocapillary flows in cylindrical liquid bridges. *J. Fluid Mech.* **2000**, *414*, 285–314.

- (67) Jiang, X.; Hou, B.; Wang, J.; Yin, Q.; Zhang, M. Model to Simulate the Structure of a Crystal Pillar and Optimize the Separation Efficiency in Melt Crystallization by Fractal Theory and Technique. *Ind. Eng. Chem. Res.* **2011**, *50* (17), 10229–10245.
- (68) Yu, B.; Cheng, P. A fractal permeability model for bi-dispersed porous media. *Int. J. Heat Mass Transfer* **2002**, *45* (14), 2983–2993.
- (69) Sahimi, M. Nonlinear transport processes in disordered media. *AIChE J.* **1993**, *39* (3), 369–386.
- (70) Civan, F. Scale effect on porosity and permeability: Kinetics, model, and correlation. *AIChE J.* **2001**, *47* (2), 271–287.
- (71) Yu, B.; Liu, W. Fractal analysis of permeabilities for porous media. *AIChE J.* **2004**, *50* (1), 46–57.
- (72) Cai, J.; Yu, B. A Discussion of the Effect of Tortuosity on the Capillary Imbibition in Porous Media. *Transp. Porous Media* **2011**, *89* (2), 251–263.
- (73) Cai, J.; You, L.; Hu, X.; Wang, J.; Peng, R. Prediction of effective permeability in porous media based on spontaneous imbibition effect. *Int. J. Mod. Phys. C* **2012**, *23*, (7)1250054.
- (74) Cai, J.; Perfect, E.; Cheng, C.-L.; Hu, X. Generalized Modeling of Spontaneous Imbibition Based on Hagen–Poiseuille Flow in Tortuous Capillaries with Variably Shaped Apertures. *Langmuir* **2014**, *38*, 5142–5151.
- (75) Jiang, X.; Wang, J.; Hou, B.; He, G. Progress in the application of fractal porous media theory to property analysis and process simulation in melt crystallization. *Ind. Eng. Chem. Res.* **2013**, *52* (45), 15685–15701.
- (76) Fukui, K.; Maeda, K.; Kuramochi, H. Melt crystallization for refinement of triolein and palmitic acid mixture as a model waste oil for biodiesel fuel production. *J. Cryst. Growth* **2013**, *373*, 102–105.
- (77) Nishimura, K.; Maeda, K.; Kuramochi, H.; Nakagawa, K.; Asakuma, Y.; Fukui, K.; Osako, M.; Sakai, S.-i. Solid–Liquid Equilibria in Fatty Acid/Triglycerol Systems. *J. Chem. Eng. Data* **2011**, *56* (4), 1613–1616.
- (78) Fukui, K.; Maeda, K. Distribution of solute at solid–liquid interface during solidification of melt. *J. Chem. Phys.* **1998**, *109* (17), 7468.
- (79) Wei, H. Y. D. L. P. Method for purifying phosphoric acid solution by crystallization. Chin. Pat. 1730385A Feb. 8, 2006.
- (80) Wang, J. J. X.; Hou, B.; Zhang, M.; Yin, Q.; Bao, Y.; Wang, Y.; Gong, J., Static multiple-stage melt crystallization process for preparing electronic grade phosphoric acid. Chin. Pat. 102198937A Sep. 28, 2011.
- (81) Wang, J. J. X.; Hou, B.; Zhang, M.; Yin, Q.; Bao, Y.; Wang, Y.; Gong, J., Preparation method of electronic grade phosphoric acid by liquid film crystallization Chin. Pat. 101774555A Jul. 14, 2010.
- (82) Rich, A.; Mandri, Y.; Bendaoud, N.; Mangin, D.; Abderafi, S.; Bebon, C.; Semlali, N.; Klein, J.-P.; Bounahmidi, T.; Bouhaouss, A. Freezing desalination of sea water in a static layer crystallizer. *Desalin. Water Treat.* **2010**, *13* (1–3), 120–127.
- (83) Kumashiro, M.; Izumi, Y.; Hoshino, T.; Fujita, Y.; Hirasawa, I. Purification of Aluminum Nitrate Nonahydrate by Melt Crystallization. *J. Chem. Eng. Jpn.* **2011**, *44* (2), 105–109.
- (84) Choi, J.-H.; Cho, Y.-Z.; Lee, T.-K.; Eun, H.-C.; Kim, J.-H.; Kim, I.-T.; Park, G.-I.; Kang, J.-K. Inclusion behavior of Cs, Sr, and Ba impurities in LiCl crystal formed by layer-melt crystallization: Combined first-principles calculation and experimental study. *J. Cryst. Growth* **2013**, *371*, 84–89.
- (85) Rauls, E.; Wiebe, J.; Schmidt, W. Understanding the cubic AlN growth plane from first principles. *J. Cryst. Growth* **2010**, *312* (20), 2892–2895.
- (86) David, D.; Guerreiro, J.; da Silva, M.; Castro Meira, M.; Bargiela, P.; de Almeida, J.; Freitas, J., Jr.; Ferreira da Silva, A. Properties of nitrogen-doped titanium oxides. *J. Cryst. Growth* **2012**, *350* (1), 11–16.
- (87) Fu, Y. P.; Wen, S. B.; Lu, C. H. Preparation and Characterization of Samaria-Doped Ceria Electrolyte Materials for Solid Oxide Fuel Cells. *J. Am. Ceram. Soc.* **2008**, *91* (1), 127–131.
- (88) Chandrapala, J.; Oliver, C. M.; Kentish, S.; Ashokkumar, M. Use of power ultrasound to improve extraction and modify phase transitions in food processing. *Food Rev. Int.* **2013**, *29* (1), 67–91.
- (89) Sato, K.; Ueno, S. Crystallization, transformation and microstructures of polymorphic fats in colloidal dispersion states. *Curr. Opin. Colloid Interface Sci.* **2011**, *16* (5), 384–390.
- (90) Suzuki, A.; Lee, J.; Padilla, S.; Martini, S. Altering functional properties of fats using power ultrasound. *J. Food Sci.* **2010**, *75* (4), E208–E214.
- (91) Liang, X. M., Y.; Yang, Y.; Xiao, Y.; Li, D.; Zhao, H.; Wu, L.; Wang, R., Method for preparation of high-purity phosphoric acid by flowing chromatographic crystallization. Chin. Pat. 101759167A, Jun. 30, 2010.
- (92) Qin, J.; Shi, W.; Yang, H.; Liu, J.; Yu, J.; Lv, Q.; Tian, Y. Sonochemical activation calcium sulfate whisker with enhanced beta-nucleating ability for isotactic polypropylene. *Colloid Polym. Sci.* **2013**, *291* (11), 2579–2587.
- (93) Ubbenjans, B.; Frank-Rotsch, C.; Virbulis, J.; Nacke, B.; Rudolph, P. Numerical analysis of the influence of ultrasonic vibration on crystallization processes. *Cryst. Res. Technol.* **2012**, *47* (3), 279–284.
- (94) Chen, P.; Chen, X. D.; Free, K. W. An experimental study on the spatial uniformity of solute inclusion in ice formed from falling film flows on a sub-cooled surface. *J. Food Eng.* **1999**, *39* (1), 101–105.
- (95) Delgado, A. E.; Zheng, L.; Sun, D.-W. Influence of ultrasound on freezing rate of immersion-frozen apples. *Food Bioprocess Technol.* **2009**, *2* (3), 263–270.
- (96) Alizadeh, E.; Chapleau, N.; de-Lamballerie, M.; Le-Bail, A. Impact of freezing process on salt diffusivity of seafood: Application to salmon (*salmo salar*) using conventional and pressure shift freezing. *Food Bioprocess Technol.* **2009**, *2* (3), 257–262.
- (97) Fuchigami, M.; Kato, N.; Teramoto, A. High-Pressure-Freezing Effects on Textural Quality of Carrots. *J. Food Sci.* **1997**, *62* (4), 804–808.
- (98) Moreno, F. L.; Hernándezb, E.; Raventós, M.; Robles, C.; Ruiz, Y. A process to concentrate coffee extract by the integration of falling film and block freeze-concentration. *J. Food Eng.* **2014**, *128*, 88–95.
- (99) Hottot, A.; Vessot, S.; Andrieu, J. A direct characterization method of the ice morphology. Relationship between mean crystals size and primary drying times of freeze-drying processes. *Drying Technol.* **2004**, *22* (8), 2009–2021.
- (100) Kiani, H.; Sun, D.-W. Water crystallization and its importance to freezing of foods: A review. *Trends Food Sci. Technol.* **2011**, *22* (8), 407–426.